Quaternary Science Reviews 385 (2026) 110012

Contents lists available at ScienceDirect

Quaternary Science Reviews

journal homepage: www.elsevier.com/locate/quascirev

Cliff-top boulder deposits as geomorphological markers of Last Interglacial extreme wave events in the Mediterranean: evidence from south-eastern Sicily

Giovanni Scardino [a,*], Alessio Rovere [b,c], Mario Marcello Miglietta [d], Tommaso Alberti [a], Alok Kushabaha [e], N.A.K. Nandasena [f], Marco Anzidei [a], Giovanni Scicchitano [g]

[a] Istituto Nazionale di Geofisica e Vulcanologia, Roma, Italy
[b] Department of Environmental Sciences, Informatics and Statistics, Ca' Foscari University of Venice, Venezia, Italy
[c] MARUM, Center for Marine Environmental Sciences, University of Bremen, Bremen, Germany
[d] Institute of Atmospheric Sciences and Climate (CNR-ISAC), National Research Council of Italy, Padua, Italy
[e] IUSS - School for Advanced Studies, Pavia, Italy
[f] Civil and Environmental Engineering Department, United Arab Emirates University, Al Ain, 15551, United Arab Emirates
[g] Department of Earth and Geoenvironmental Sciences, University of Bari Aldo Moro, Bari, 70125, Italy

ARTICLE INFO

Handling editor: Biagio Giaccio

Keywords:
Marine deposits
Warmer sea
Sea-level projections
Medicane
Tsunami

ABSTRACT

Cliff-top boulder deposits represent one of the most extreme and debated geomorphological expressions of high-energy coastal processes, as their emplacement requires sustained overtopping of cliffs during coastal flooding. Occurring several metres above mean sea level and well beyond the reach of ordinary wave run-up, cliff-top boulder deposits are particularly sensitive indicators of extreme wave events. In this study, we investigate cliff-top boulder deposits atop a 10-m-high cliff in south-eastern Sicily by integrating geomorphological observations with hydrodynamic modelling for both present and Last Interglacial forcing conditions. Hydrodynamic modelling was used to simulate extreme wave events that can cause coastal flooding and wave flow under tropical-like cyclone and tsunami scenarios. To evaluate the geomorphological effects of these extreme wave events, we modelled and compared the current scenarios under the present-day sea level, and Last Interglacial scenarios, which in contrast, incorporate elevated relative sea level and intensified hurricane and tsunami forcings to evaluate wave flow needed for cliff-top deposit emplacement. The results reflect a scenario with a Last Interglacial post-highstand regressive phase, highlighting the role of sea-level-controlled boundary conditions in enabling extreme coastal flooding and inland boulder transport. Our results indicate that Mediterranean cliff-top boulder deposits reflect the effectiveness of extreme waves acting under specific boundary conditions, rather than the absolute magnitude of the waves themselves, with relative sea level exerting a first-order control on coastal impact.

1. Introduction

Coastal boulder deposits represent key geomorphological archives for reconstructing the occurrence, magnitude, and recurrence of past high-energy coastal events such as storms and tsunamis (Cox et al., 2020; Goto et al., 2010; Kennedy et al., 2021, 2025; Kortekaas and Dawson, 2007; Minamidate and Goto, 2024). However, the geomorphological significance of coastal boulder deposits is strongly dependent on their depositional setting, elevation, and relationship with coastal morphology, which control both their emplacement mechanisms and their preservation potential. Several studies have revealed these features along the North Atlantic coasts, where long-term monitoring was performed on storm-induced boulder transportation (Autret et al., 2017, 2023; Cox et al., 2019; Suanez et al., 2026). In particular, the interpretation of coastal boulders from Pleistocene highstands, such as the Last Interglacial (LIG), remains challenging due to subsequent erosion, reworking, and overprinting by later sea-level oscillations (Ruban, 2019; Marriner et al., 2017). Within this broad category, cliff-top boulder deposits (CTBDs) represent one of the most extreme and debated geomorphological expressions of high-energy coastal processes. Unlike

* Corresponding author.
E-mail address: giovanni.scardino@ingv.it (G. Scardino).

https://doi.org/10.1016/j.quascirev.2026.110012
Received 20 January 2026; Received in revised form 7 April 2026; Accepted 20 April 2026

coastal boulders emplaced on shore platforms, beaches, or low-elevation coastal plains, CTBDs are located atop coastal cliffs, often several metres above mean sea level and well beyond the reach of ordinary wave run-up (Cox, 2020; Cox et al., 2018; Hall et al., 2006; Watanabe et al., 2019; Williams and Hall, 2004). Their emplacement, therefore, requires not only large wave heights but also exceptional hydrodynamic conditions typical of the higher sea level during the Last Interglacial—conditions capable of overtopping cliffs and sustaining high flow velocities across subaerial surfaces (Watanabe et al., 2019)—making CTBDs particularly sensitive indicators of extreme coastal flooding. Furthermore, atmospheric and oceanographic conditions in the Mediterranean basin during the Last Interglacial should have determined intensified tropical-like cyclones, with higher wave heights and flow velocities capable of producing greater wave setup and runup along the cliffs, also considering different tide phases (Autret et al., 2016; Fichaut and Suanez, 2011).

CTBDs have been documented worldwide along high-energy coastlines in the Atlantic (Cox et al., 2018; Dunán-Avila et al., 2024; Etienne and Paris, 2010; Hall et al., 2006; Hansom and Hall, 2009; Noormets et al., 2004; Pedoja et al., 2023; Rovere et al., 2017), the Mediterranean (Biolchi et al., 2016; Causon-Deguara et al., 2025; Corradino et al., 2025; Delle Rose, 2024; Korbar et al., 2022; Maouche et al., 2009; Nadia Mhammdi et al., 2008; Roig-Munar et al., 2019), and the Pacific (Bourrouilh-Le Jan and Talandier, 1985; Canavesio et al., 2023; Köhler et al., 2025), where they are typically characterised by large boulder volumes, significant inland transport distances, and preferential accumulation near cliff edges or along low-roughness pathways. Because of these characteristics, CTBDs are commonly regarded as proxies for the upper bounds of coastal wave energy. However, their genetic interpretation remains controversial (Cox et al., 2020; Goto et al., 2010; Kennedy et al., 2021). Tsunamis have traditionally been considered the most plausible mechanism for CTBD emplacement, owing to their long wavelengths, sustained flow depths, and capacity to generate cliff-overtopping inundation. More recently, observational evidence and numerical modelling have shown that storm waves may also be capable of emplacing TCBDs under higher sea-level conditions, where favourable cliff geometry and reduced surface roughness act to amplify wave run-up and inland flow velocities (Dewey and Ryan, 2017; Hall et al., 2006; Rovere et al., 2017, 2026).

In the semi-enclosed basins, such as the Mediterranean Sea, present-day storms are generally less intense than those affecting open-ocean margins due to limited fetch, smaller storm size, and reduced maximum wave heights. As a result, the occurrence of CTBDs along Mediterranean rocky coasts cannot be straightforwardly attributed to exceptionally intense storms comparable to oceanic “superstorms” that occurred in the Last Interglacial (Hansen et al., 2016; Hearty, 1997; Hearty and Tormey, 2017). Instead, Mediterranean CTBDs are more plausibly interpreted as the result of boundary-condition amplification, whereby moderate-to-strong storms or tsunamis become geomorphologically effective only when coupled with elevated relative sea level. Periods characterised by higher sea level, such as the Last Interglacial, would have significantly reduced the vertical distance between wave base and cliff tops, increasing the likelihood of cliff overtopping, sustained coastal flooding, and inland transport of large boulders.

From this perspective, CTBDs do not necessarily record anomalously large waves alone, but rather the combined effect of wave energy and boundary conditions, with relative sea level acting as a first-order control on coastal impact. Consequently, CTBDs in the Mediterranean basin may represent valuable geomorphological archives of extreme coastal events preferentially occurring during warm-climate intervals, when elevated sea level fundamentally altered coastal wave dynamics. In this sense, Last Interglacial CTBDs offer a robust framework for investigating the geomorphological response of rocky coastlines to extreme events and provide a process-based analogue for assessing future coastal hazards under ongoing sea-level rise.

In this study, we focus on CTBDs located at Capo Muro di Porco in south-eastern Sicily, a rocky coastal sector exposed to both seismic and atmospheric hazards, including Mediterranean hurricanes. We integrate detailed geomorphological observations with hydrodynamic modelling under both current (1995-2025 CE) and Last Interglacial (LIG, 129–116 ka) boundary conditions. Current scenarios are used as process baselines to evaluate the geomorphological effectiveness of extreme wave events under present-day sea-level conditions, whereas intensified hurricane and tsunami forcings combined with elevated relative sea level are applied to LIG scenarios to assess the conditions required for CTBD emplacement. Through this approach, we evaluate whether the CTBDs at Capo Muro di Porco can be interpreted as geomorphological markers of extreme wave events associated with LIG boundary conditions in the Mediterranean basin.

This paper begins by investigating the atmospheric and oceanographic conditions that characterized the Mediterranean Sea during the LIG (Section 1.1). We then turn our focus to southeastern Sicily, presenting its geological and geomorphological framework—with particular attention to the Capo Muro di Porco —in Section 2. Section 3 outlines the materials and methods used to model extreme wave events, specifically cyclones and tsunamis, under both present and LIG conditions. The core findings from these simulations are detailed in Section 4, followed by a discussion of their broader implications in Section 5. Ultimately, we conclude (Section 6) that the CTBDs at Capo Muro di Porco serve as a unique geomorphological fingerprint, preserving the signature of extreme wave events that impacted the Mediterranean during the Last Interglacial.

1.1. *Atmospheric and oceanographic variables in the Mediterranean basing during the last interglacial*

Here, we refer to LIG as the Marine Isotope Stage (MIS) 5e, spanning approximately 129 to 116 thousand years ago (ka). This was the most recent geological period characterized by a climate slightly warmer than the pre-industrial (Hoffman et al., 2017; Lang and Wolff, 2011; Obreht et al., 2022; O'ishi et al., 2021; Otto-Bliesner et al., 2013; Turney et al., 2020). Global mean annual sea surface temperature (SSTs) during the LIG peaked at levels warmer than the 1870–1889 climatological mean (Hoffman et al., 2017). Within the Mediterranean basin, paleoceanographic data from marine cores (Fig. 1) highlighted that LIG SSTs were consistently higher than late-Holocene temperatures (Dixit et al., 2020; Martrat et al., 2004, 2014). Specifically, the Western Mediterranean exhibited large annual SST anomalies (difference between interglacial optimum and preceding glacial maximum, MIS 6) ranging from 7 °C to 10 °C (Davtian et al., 2019), with the Gulf of Lions showing anomalies up to 10 °C. Reconstructions from the Eastern Mediterranean suggest a considerable SST increase from 125 ka (Obreht et al., 2022). One high-resolution record indicates an abrupt SST increase of 3.6 °C in approximately 100 years (between 125.67 and 125.57 ka) (Obreht et al., 2022, 2025). This warming trend coincided with strong stratification, allowing heat gained at the surface to be trapped, and consequently, large SST variations were controlled by changes in the mixed layer depth (Amies et al., 2019; Marino et al., 2007; Obreht et al., 2022).

The most prominent feature of the LIG Mediterranean climate was a profound change in the basin's freshwater budget, leading to the deposition of organic-rich sapropel layer S5 (~128.3–121.5 ka) (Amies et al., 2019; Cane et al., 2002; Rohling et al., 2004, 2006). The timing of S5 coincided with precession minima, which are associated with the northward migration and intensification of the monsoon rain belt over North Africa (Amies et al., 2019; Grant et al., 2016; Heslop et al., 2023; Huang et al., 2021). The resulting increase in monsoon precipitation over the Sahara drove a large influx of low-freshwater runoff into Eastern Mediterranean surface waters (Amies et al., 2019; Tisserand et al., 2009). Model results highlighted that African monsoon runoff increased substantially, reaching levels up to ~8.8 times the modern pre-Aswan Nile discharge (Amies et al., 2019). This freshwater injection caused negative anomalies recorded in planktic foraminiferal calcite (Rohling et al., 2004). The actual onset of S5 deposition (~128.3 ka)

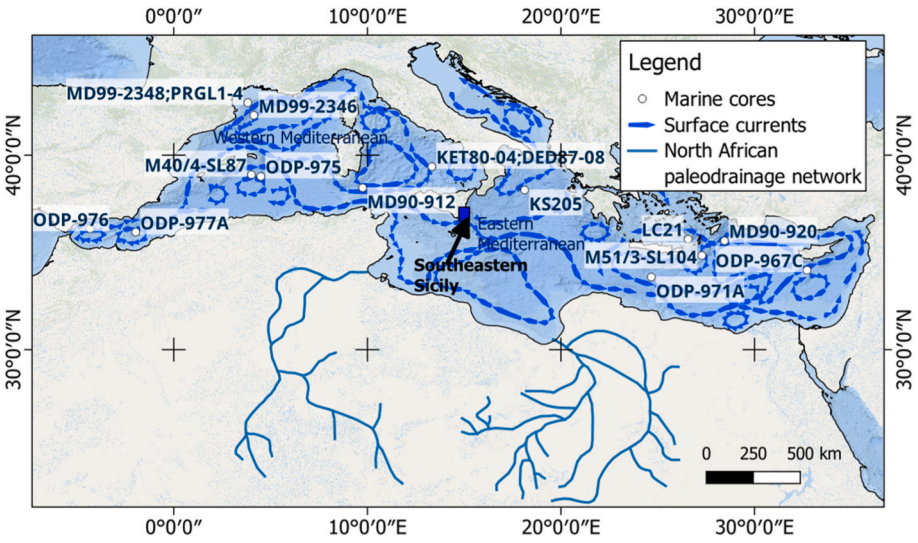

Fig. 1. – Regional scale framework of Mediterranean Sea; marine core locations derived from literature works that considered the paleo-oceanographic variables during LIG (details in the Supplementary Material S1); surface currents derived from work of (Pinardi et al., 2015) (representing 1987–2007 time-mean circulation at 15 m depth); while North African paleodrainage network was summarized by works of Rohling et al. (2002); Osborne et al. (2008); Amies et al. (2019).

followed the estimated increase in monsoon intensity (~128.5 ka) by about 200 years, implying a rapid preconditioning of the eastern Mediterranean for sapropel formation(Amies et al., 2019; Rohling et al., 2004, 2006).

The rapid addition of large volumes of freshwater led to strong density stratification of the water column, causing the pycnocline and nutricline to shoal (Incarbona et al., 2022; Obreht et al., 2022). This weakening of dense water formation resulted in oxygen starvation at depth (Incarbona et al., 2022). In the Aegean Sea, ventilation is inferred to have collapsed completely within 40 ± 20 years of the onset of surface freshening, despite the primary hydrological change being centred on the open Eastern Mediterranean basin (Marino, 2008; Marino et al., 2007). Euxinic conditions (indicated by isorenieratene, a marker for photic zone anoxia) subsequently expanded through the Aegean water column up to 200m or less and reached the open Eastern Mediterranean ~100–300 years later (Marino et al., 2007).

In the Western Mediterranean and its northern borderlands, the MIS 5e was also characterized by enhanced moisture availability (Dixit et al., 2020). Geochemical data from the northern Tyrrhenian Sea indicate high river discharge and lower Sea Surface Salinity during MIS 5e, resulting from enhanced winter rainfall (Dixit et al., 2020; Gao et al., 2025; Kallel et al., 2004). The winter's precipitation variability was primarily influenced by the North Atlantic atmospheric circulation (Dixit et al., 2020). This synchronous pattern—of heightened winter runoff in the west and intensified summer monsoonal rainfall and carbon deposition in the east—reveals a closely coupled low- and high-latitude climate system that collectively generated anoxic conditions throughout the Mediterranean basin (Rohling et al., 2006). The early LIG (ca. 127 ka) experienced a decrease in deep water oxygenation followed by episodes of severely reduced North Atlantic Deep Water formation, indicating a weakened Atlantic Meridional Overturning Circulation (Hayes et al., 2014; Levy et al., 2023). A mid-LIG cooling decrease (ca. 126 ka to ca. 122 ka) recorded in speleothems in the Levant basin suggested an atmospheric circulation reorganization, potentially involving increased moisture uptake from the central and western Mediterranean due to heightened air flow from the North Atlantic (Levy et al., 2023).

2. Geological and geomorphological settings

The Maddalena Peninsula, encompassing the Capo Muro di Porco area along the Ionian coast is located within the Hyblean Plateau of southeastern Sicily (Bianca et al., 1999; Meschis et al., 2020; Monaco et al., 2002; Westaway, 1993). The Hyblean plateau represents the emergent foreland of the Sicilian-Maghrebian domain (Fig. 2a), forming part of the African Pelagian Block (Bianca et al., 1999; Cultrera et al., 2015; Henriquet et al., 2019, 2021; Westaway, 1993). From a structural point of view, the peninsula is identified as a calcareous horst dipping gently towards the East-Northeast (Viger et al., 2024; Westaway, 1993). The lithostratigraphic succession includes Miocene limestones overlain by Pleistocene calcarenites (Cultrera et al., 2015; Grasso and Lentini, 1982; Meschis et al., 2020; Scicchitano et al., 2016). The active deformation observed in this region is primarily linked to the large system of normal faults related to the Malta Escarpment (MESC), a regional structural boundary that has been active since the Middle Pleistocene (Argnani et al., 2012; Argnani and Bonazzi, 2005; Azzaro and Barbano, 2000; Bianca et al., 1999; Gambino et al., 2022; Piatanesi and Tinti, 1998). As a consequence, the coastal zone is marked by multiple sequences of uplifted paleoshorelines and marine terraces (Dutton et al., 2009; Meschis et al., 2020; Scicchitano et al., 2016; Scicchitano and Monaco, 2006). Both contemporary and ancient coastal cliffs are frequently associated with karst levels (including caves, channels, and siphons) incised within the carbonate rock sequence (Bianca et al., 1999; Scardino et al., 2022a; Scicchitano and Monaco, 2006; Varzi et al., 2024).

The Maddalena Peninsula coastline is characterized by the widespread occurrence of coastal boulder fields (Scicchitano et al., 2007, 2012, 2020). These boulders are scattered across an extensive Pleistocene abrasion platform located between 5 and 15 m above sea level (Fig. 2b) (Scicchitano et al., 2008, 2012). The platform gradually slopes toward the sea and is generally bordered by coastal cliffs reaching up to 5-10 m in height (Fig. 2c and d) (Scicchitano et al., 2012; Spampinato et al., 2011). The largest boulders, weighing up to 50 tons, tend to accumulate preferentially on promontories exposed to the northeast, sometimes located up to 70 m inland from the modern coastline (Scicchitano et al., 2007, 2008).

The mobilization and deposition of these boulders have been correlated with the impact of extreme wave events (Nandasena et al., 2022; Scicchitano et al., 2007). Hydrodynamic equations, combined with radiocarbon dating of marine organisms encrusting the blocks, suggest that the heavier and larger boulders were transported by tsunami waves generated by historical seismic events (e.g., 1169, 1693, and 1908) (Scicchitano et al., 2007, 2008, 2010). Specifically, displacement evidence has been documented in an ancient Greek quarry located in the

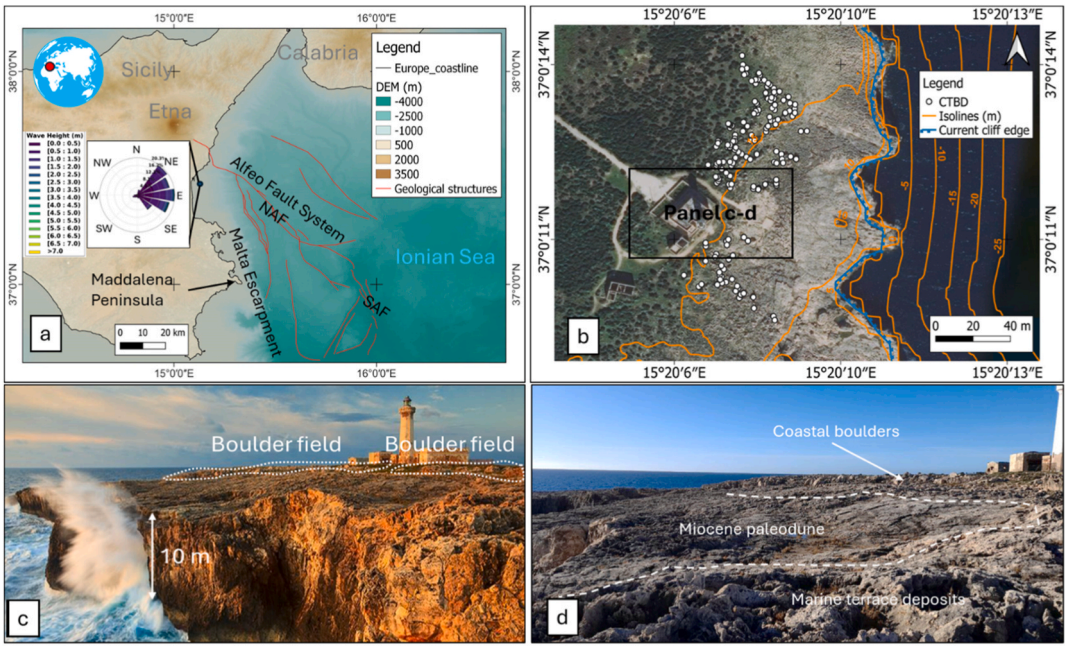

Fig. 2. – Geological features of southeastern Sicily; a) main tectonic structures of Western Ionian basin. NAF, North Alfeo Fault; SAF, South Alfeo Fault, (modified after Gambino et al., 2021), wave rose are extracted from Catania buoy data (managed by ISPRA); b) area of Capo Muro di Porco in Peninsula Maddalena with locations of coastal boulders surveyed in this study; c) cliff of Capo Muro di Porco highlighting the boulder field locations; d) evidence of marine terrace deposits overlaying the Miocene paleodune.

northern sector of the peninsula (Scicchitano et al., 2012, 2020). While intense storms (such as the 2009 event) were capable of moving large blocks (up to approximately 41 tons) (Kushabaha et al., 2024; Scicchitano et al., 2020), the largest boulders are considered remnants of tsunami events. Direct witness provided useful insights for the impact of extreme weather systems, like Mediterranean hurricanes (aka medicane), which represent mesoscale cyclones that develop over the Mediterranean Sea and display tropical-like cyclone (TLC) characteristics (Miglietta et al., 2025). Video analysis conducted during medicane Zorbas (26-29 September 2018) in the flooded Greek quarry of Peninsula Maddalena demonstrated that smaller boulders (ranging between 1 and 2 tons) were displaced via turbulent flow, reaching velocities up to 4 m/s (Nandasena et al., 2022; Scardino et al., 2022b; Scicchitano et al., 2020). These movements were attributed to the impact of multiple waves under submerged conditions, rather than a single catastrophic wave. This coastal stretch is characterized by micro-tidal tides with a range between 0.1 and 0.3 m (Braitenberg et al., 2011;McDonagh et al., 2024). Typically, the impact related to TLCs and seasonal storms results in a temporary increase in water levels, which is reflected in extended inland (Scardino et al., 2022b;Scicchitano et al., 2021).

Global eustatic sea-level estimates for the MIS 5e is generally attributed to 6 ± 3 m in stable areas (Dutton and Lambeck, 2012; Ferranti et al., 2006; Hearty et al., 2007; Maxwell et al., 2021). The sea-level position during the MIS 5e highstand in southeastern Sicily is recorded at various elevations due to the region's differential uplift pattern (Dutton et al., 2009; Meschis et al., 2020; Spampinato et al., 2013; Varzi et al., 2024). Also the area of Capo Muro di Porco experienced differential vertical land movements, with measured uplift rates typically decreasing from north to south (Anzidei et al., 2021; Meschis et al., 2020; Viger et al., 2024). Here, marine terrace deposits attributed to MIS 5e are extended from 10 m to 27 m of elevation, overlaying Miocene paleodune deposits (Meschis et al., 2020; Scicchitano et al., 2016; Spampinato et al., 2011)(Spampinato et al., 2012).

Paleo-sea level markers provide essential chronological constraints for quantifying the tectonic deformation in this area (Scicchitano et al., 2016; Spampinato et al., 2011, 2012, 2013). The Akradina Terrace, located near Siracusa, provides critical evidence, with its inner edge mapped at +32 m (Bianca et al., 1999; Cosentino and Gliozzi, 1992; Lambeck et al., 2004). Based on current interpretations, this terrace is correlated with either MIS 5c or, less likely, MIS 5e (Antonioli et al., 2006; Ferranti et al., 2006). If attributed to MIS 5c, this suggests an uplift rate of around 0.25 mm/a (Meschis et al., 2020). The underwater geomorphology along the coast between Capo Santa Panagia and Ognina (near the Maddalena Peninsula) displays at least two submerged paleo-cliffs, found roughly between −9 and −22 m, and between −20 and −45 m depth (Dutton et al., 2009; Scicchitano and Monaco, 2006; Spampinato et al., 2011). U/Th dating of speleothems within the submerged caves and 14C dating of encrusting serpulid layers from the Plemmirio Cave (located at −20.22 m depth on the Maddalena Peninsula) provide critical age constraints (Dutton et al., 2009; Ferranti et al., 2010; Scicchitano and Monaco, 2006), with clusters of U-Th ages spanning from 72.4 ± 0.8 ka to 76.5 ± 1.3 ka (Dutton et al., 2009). This evidence suggests that the submerged paleo-shoreline detected at approximately −20 m depth is attributable to the MIS 5a substage (~76.5 ka or 80.0 ka). The combined use of submerged and terrestrial markers consistently indicates a long-term average uplift rate of 0.2 to 0.4 mm/a in the Siracusa region over the last glacial–interglacial cycle. This uplift is due to regional geodynamic processes acting in concert with the activity of the offshore geological structures (Bianca et al., 1999; Gambino et al., 2021, 2022; Meschis et al., 2020).

At Capo Muro di Porco, the studied CTBDs consist of a field of large calcarenite boulders emplaced on the cliff-top surface 10 m above the present-day shoreline. The boulders are located several metres above mean sea level (msl), ranging from 12 to 15 m of altitude, and lie well beyond the reach of ordinary wave run-up under present-day conditions (Inghilesi et al., 2000), implying emplacement by cliff overtopping and sustained coastal flooding. Wave data from the Catania buoy (RON—Rete Ondametrica Nazionale; www.idromare.com), covering the last 18 years along the Ionian coast of Sicily, provide significant spectral wave height (Hm0) and peak period (Tp) measurements. The most severe storm recorded occurred on 2 February 1996, characterized by an Hm0 of about 6.2 m and a Tp of 11.3 s (Scicchitano et al., 2020). Furthermore, boulder elevations are also higher than the estimated runup of historical tsunamis, which reached up to 5 m above msl (Billi

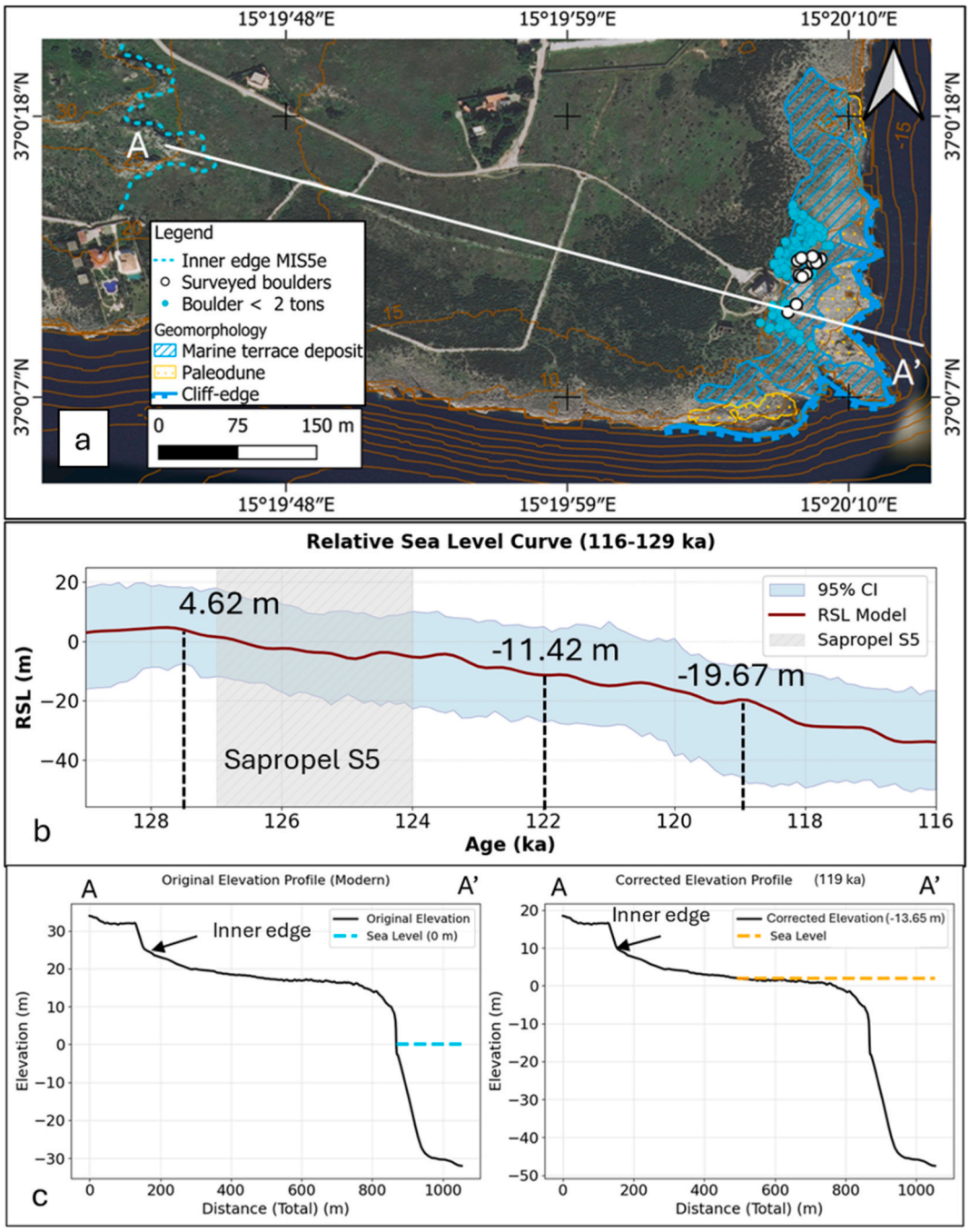

Fig. 3. – Geomorphological and topographic features of Capo Muro di Porco; a) location of surveyed boulders and coastal landforms (map was realized through QGIS software); b) Grant et al. (2014) sea-level curve, the temporal range of sapropel S5 deposition is highlighted in gray, while the dashed black lines indicate the temporal constraints considered for the paleo-landscape reconstruction (see Table 2); c) current topographic profile reporting present-day elevations and sea level (dashed cyan line) and d) corrected topographic profile for a vertical displacement of −13.65 m corresponding to corrected LIG sea level for Capo Muro di Porco site. (For interpretation of the references to colour in this figure legend, the reader is referred to the Web version of this article.)

et al., 2009; Scicchitano et al., 2022). The deposit is discontinuous and spatially organized, with 166 CTBDs extending from 40 to 104 m from the cliff edge along a pathway characterized by relatively low surface roughness. This pathway corresponds to the Miocene palaeodune cropping out on the cliff-top surface, which provides a smoother substrate compared to the surrounding marine deposits.

The boulders composing the deposit are lithologically consistent with the marine terraced deposits and occur as isolated blocks rather than as a continuous ridge. Local imbrication of boulders is occasionally observed. Their spatial arrangement does not show evidence of constructional features typical of talus accumulation or gravitational collapse from the cliff face. On the other hand, the paleo-cliff corresponding to the LIG highstand is located about 600 m landward of the current cliff edge. The observed distribution suggests inland transport across the cliff-top surface following overtopping events, with boulder positions controlled by local topography and surface roughness.

No comparable cliff-top boulder deposits have been identified in the surrounding coastal sectors or elsewhere along the rocky coasts of insular Sicily (Causon Deguara and Gauci, 2017; Scicchitano et al., 2007, 2012, 2020).

No historical or instrumental records exist of storm- or tsunami-induced cliff overtopping that could emplace such a deposit under

present-day relative sea-level (RSL) conditions. This lack of modern analogues, together with the elevation and spatial arrangement of the boulder field, suggests that its emplacement required boundary conditions different from those that characterised the Holocene.

3. Material and methods

This work combines morpho-topographic surveys at Capo Muro di Porco with hydrodynamic modelling to reconstruct wave flow conditions for different extreme wave scenarios during LIG, focusing on medicanes and tsunamis. The methodology considered the development of a present-day Digital Elevation Model (DEM) and Terrestrial Laser Scanner (TLS) survey to assess the dimensional features of CTBDs. These dimensional features represent an important insight for the reproducibility of data related to coastal boulder studies(Cox et al., 2025). Using the dimensional data from the TLS, the minimum wave flow necessary to initiate boulder transport was estimated via incipient motion equations (Nandasena et al., 2022). The wave flow values obtained through incipient motion represent the threshold velocities for the CTBD movements. These thresholds were then evaluated against simulated wave flows from storm and tsunami models, applied to a reconstructed LIG paleo-landscape of Capo Muro di Porco. The procedural steps are outlined below:

1 Morpho-topographic surveying and boulder characterization at Capo Muro di Porco;
2 Specification of forcing conditions for medicanes and tsunamis;
3 Cyclone intensity modeling (Lin et al., 2023 model);
4 Earthquake-generated tsunami modeling (Okada-Delft3D model suite);
5 Morphodynamic modeling of medicanes and tsunamis (XBeach model).

3.1. Morpho-topographic surveys through terrestrial laser scanner and LiDAR in Capo Muro di Porco

We used a Faro Focus X130 terrestrial laser scanner to measure the dimensions of the CTBDs on the Capo Muro di Porco cliff (Fig. 3). Ground control points (GCPs) were measured along the cliff using an EMLID RS3+ differential GNSS receiver. GCP measurements were corrected in post-processing considering the base stations of the *Rete Integrata Nazionale GPS* (RING) and HxGN SmartNet networks (managed by Hexagon). The collected ellipsoid elevations were converted into geodetic elevations referenced to Earth Gravitational Model (EGM) 2008 (Pavlis et al., 2012). We then extrapolated the "ab" and "ac" surfaces of each CTBD following the approach described by Nandasena et al. (2022) and reported in other studies (Dunán-Avila et al., 2024; Engel et al., 2025; Scardino et al., 2025). These surfaces were converted to meshes and translated to planar projections to determine their areas and axial lengths ($a > b > c$). Finally, the actual volumes of each boulder were calculated in CloudCompare software. To calculate the minimum flow velocities required to move each boulder, we applied the incipient-motion formulas, using the coefficients shown in Table 1. Among the pre-transport conditions reported in Nandasena et al. (2022), we only calculated threshold velocities for submerged or subaerial isolated boulders, joint-bounded boulders, and cliff-edge, which represent the only pre-setting conditions detectable in the field.

Table 1
Coefficients used to calculate the minimum flow velocity to transport boulders.

Coefficients	Values
Drag	1.5
Lift	0.7
Static friction	0.5
Bed angle	1.2°

The LIG paleo-landscape of Capo Muro di Porco was reconstructed considering the published horizontal limestone-lowering rate for this area, which was estimated equal to 0.14 mm/a (Furlani and Cucchi, 2013; Scardino et al., 2022a; Scicchitano et al., 2016). This limestone lowering rate, applied over a period extending to 119 ka, is reflected in a cliff edge that lies more than 16 m farther seaward than the present one. A seaward buffer extending 16 m from the cliff-edge was produced in QGIS, and the LiDAR-DTM data from the Ministry of the Environment and Energy Security (MASE) was corrected with geodetic elevations of EGM 2008 and modified to project the cliff edge to the seaward limit of this buffer. The modified LiDAR-DTM was extracted with 2×2 m cell width and a mean vertical resolution of about 20 cm. To model the changes of the local topography at the LIG period, elevations on LiDAR-DTM cells were corrected with the RSL of LIG period. The assessment of RSL of the LIG period was performed considering the sea-level curve from Grant et al. (2014), the displacements of uplift rates reported by Meschis et al., (2020), and Glacial Isostatic Adjustment (GIA) from Stocchi et al. (2018). Grant et al. (2014) reported a sea-level value of −19.6 m for 119 ka. In contrast, the elevation of the marine terrace attributed to the same period was found to be 16 m (Meschis et al., 2020). This was inferred by a chronological constraint from a coral sample of *Cladocora caespitosa* collected at 14 m above msl within the marine terrace deposit yielded an age of 119 ka. Considering the GIA prediction for 122 ka, which indicated a corrected eustatic level of 4 m in the study area (following mantle viscosity profile 3 from Stocchi et al., 2018), the GIA rate at 122 ka was estimated to be 0.12 mm/a. Using this rate, the sea-level curve from Grant et al. (2014) was corrected for 127.5 ka, 122 ka, and 119 ka. Furthermore, the local tectonic uplift rate for the Maddalena Peninsula area was estimated to be 0.16 mm/a (Meschis et al., 2020). This tectonic uplift correction was then applied to the adjusted Grant et al. (2014) sea-level curve to derive the corrected LIG topography (Fig. 3) for the Capo Muro di Porco (Table 2). Following the LIG sea level, the elevations of the modified LiDAR-DTM were corrected for the value reported in column E of Table 2.

The main geomorphological features are mapped to assess the different roughness values across the cliff, in particular highlighting the difference between the low-roughness paleodunes and the high-roughness LIG marine deposits. The roughness was assessed through TLS data, using roughness tool function in CloudCompare software.

3.2. Forcings of extreme wave events: climate dataset and geological structure

Extreme wave events were simulated following three main scenarios:

1) A baseline scenario given by the medicane impact modelled under current oceanographic and atmospheric conditions for the Capo Muro di Porco site.
2) A scenario where the TLC generated the atmospheric and oceanographic anomalies during the LIG with an intensified medicane impacting the LIG paleo-landscape;
3) an earthquake-generated tsunami over the LIG paleo-landscape.

The medicane scenario used as a baseline is medicane Ianos (15–20 September 2020), which impacted south-eastern Sicily on 16–17 September 2020 (Ferrarin et al., 2023). The tsunami of 1693 AD was used as the baseline scenario for earthquake-generated tsunamis impacting the same region(Scicchitano et al., 2022).

LIG-forcings for the medicane were assessed from the Paleoclimate Model Intercomparison Project Phase 4, collectively known as the PMIP4-CMIP6 ensemble model (Eyring et al., 2019; Kageyama et al., 2016, 2021)(data will be distributed through the official CMIP6 channels via the Earth System Grid Federation ESGF, https://earthsystemcog.org/projects/wip/CMIP6DataRequest). The PMIP4-CMIP6

Table 2
– Parameters considered for the LIG sea level at different times; Grant et al. (2014) curve (column A) was corrected for the contribution of GIA reported in Stocchi et al. (2018) (equal to 0.12 mm/a for scenario MVP3) (column B); adjusted Grant et al. (2014) sea-level curve represent the eustatic level corrected for the GIA (column C); displacements due to local tectonic uplift derive from the rates published in Meschis et al. (2020) (column D). LIG corrected elevation is obtained from the sum of values of columns A-B-C-D and was considered as a correction for the topography at the given year (column E).

	A	B	C	D	E
Time (ka)	Grant et al. (2014) sea-level curve (m)	Correction of GIA (Stocchi et al., 2018) (m)	Adjusted Grant et al. (2014) sea-level curve (m)	Local tectonic uplift (m)	LIG corrected elevation (m)
127.5	−5.59	15	9.41	20	29.41
122	−11.42	14.64	3.22	19.52	16.3
119	−19.67	14.28	−5.39	19.04	13.65

simulation for the LIG is defined as the Tier 1 equilibrium experiment lig127k (Huan et al., 2023; Otto-Bliesner et al., 2017). The time slice is set at 127,000 years before present (127 ka) (Otto-Bliesner et al., 2017, 2020). The experimental design specifies this point because the orbital forcing (eccentricity, obliquity, and perihelion) produces large Northern Hemisphere seasonal insolation anomalies, while minimizing the imprint of earlier deglaciation events, and assumes atmospheric greenhouse gas concentrations similar to the pre-industrial period (Marino et al., 2015; Yeung et al., 2021). Variables considered from PMIP4-CMIP6 derive from HadGEM3 model: SST; air temperature at 1000 hPa; mean sea level pressure (MSLP); specific humidity at 1000 hPa.

The medicane scenario for the LIG was developed considering the atmospheric and oceanographic variables during the occurrence of medicane Ianos extracted from ERA5 reanalysis(Hersbach et al., 2020), and calculating the anomalies of SST, Temperature at 1000 hPa, MSLP and specific humidity at 1000 hPa (Fig. 4). These anomalies were assessed using the climatology from 1995 to 2025 of ERA5 reanalysis and subtracting the climatology of PMIP4-CMIP6 for each variable (month 9 of PMIP4-CMIP6, the procedure is reported in the Supplementary Material S2). This approach is generally used in pseudo-global warming simulations (Schär et al., 1996) to estimate the impact of climate change in a specific case study (González-Alemán et al., 2023).

Forcing conditions for earthquake-generated tsunamis were extracted from one of the main faults located offshore southeastern Sicily. This fault was identified as fault segment F3 (Gambino et al., 2021), and was considered as a major active structure along the northern sector of the Malta Escarpment (MESC) offshore Eastern Sicily (Gambino et al., 2021; Trippetta et al., 2019; Wells and Coppersmith, 1994). Geometrically, F3 is typically characterized by a N352°E trend and a mean dip of 49° toward the east, extending for a length of approximately 56 km (Gambino et al., 2021; Scicchitano et al., 2022). The F3 fault segment experienced a high seismic potential, capable of generating events exceeding Magnitude 7 (Rovida et al., 2020, 2022; Trippetta et al., 2019), with empirical scaling relationships suggesting maximum expected magnitudes up to 7.97 (Gambino et al., 2021; Wells and Coppersmith, 1994). Crucially, the prevailing dip-slip kinematic component observed for F3 provides the necessary forcing condition for generating tsunamis through coseismic seafloor displacement. For the modelling of the LIG-tsunami event, F3 parameters used include a length of 56.46 km, a mean dip of 49°, and an earthquake magnitude of Mw 7.4 (Fig. 5), as reported for the 1693 AD event (Scicchitano et al., 2022). Simulations of a 4.8 m distributed dip-slip motion along the F3 fault plane predict a 2.3 m coseismic fault-scarp at the seafloor, involving 2 m of hanging-wall downthrow and 0.3 m of footwall uplift (Grezio et al., 2024).

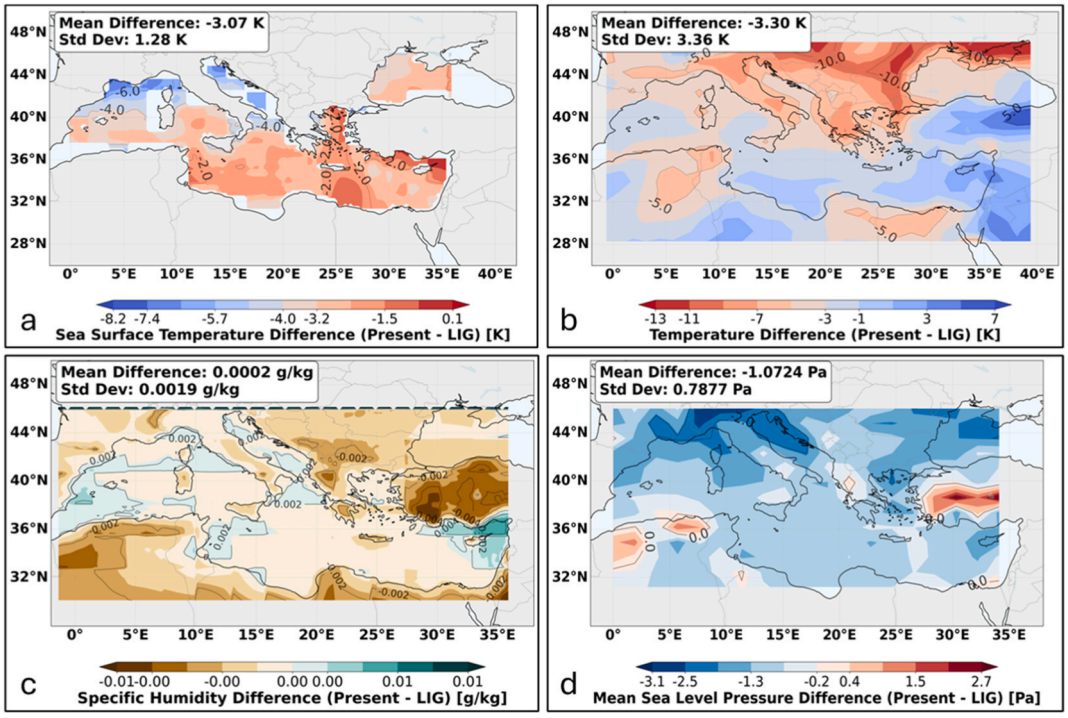

Fig. 4. Anomalies of atmospheric and oceanographic variables assessed for the medicane Ianos; a) SST spatial anomalies; b) spatial anomalies of Temperature at 1000 hPal; c) spatial anomalies of Specific Humidity at 1000 hPa; d) MSLP anomalies.

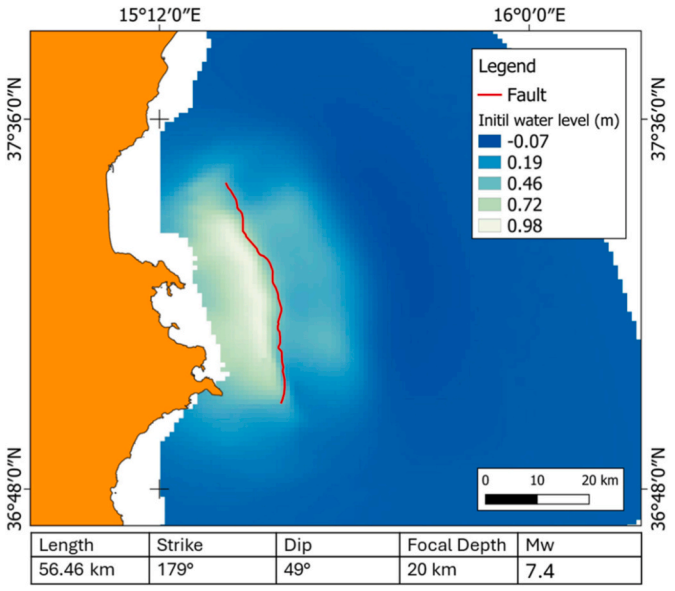

Length	Strike	Dip	Focal Depth	Mw
56.46 km	179°	49°	20 km	7.4

Fig. 5. – Initial conditions for the simulation of earthquake-generated tsunami in southeastern Sicily; fault parameters were derived from Scicchitano et al. (2022).

3.3. Modelling of cyclone intensity during the last interglacial

The assessment of medicanes intensity under the LIG scenario was performed starting from the evaluation of intensity variables and modelling the hydrodynamic response at a regional scale. To simulate the TLC intensity during the Last Interglacial, we applied the model developed by Lin et al. (2023), which is an open-source, physics-based tropical cyclone (TC) downscaling model designed to rapidly generate a large climatology of tropical cyclones and robustly sample rare events. One should note that medicanes develop mainly through a combination of baroclinic and air-sea interaction processes. When the latter dominates, the development becomes similar to that of hurricanes, possibly reaching comparable intensity and damage. Medicane Ianos, the most intense cyclone ever recorded so far, attained 1-min sustained winds of 44 m/s, similar to a category-2 hurricane. This explains why the methodology, which is proper for tropical cyclones, has been extended to consider also intense medicanes as Ianos, which behaved as tropical cyclone for part of their lifetime (Emanuel et al., 2025) .

This model uses monthly-averaged data from ERA5 reanalysis, except for the zonal and meridional winds (at 250 hPa and 850 hPa), which are substituted with daily data (details are reported in the Supplementary Material S3) to reproduce the actual cyclone track with associated maximum wind speed values for each point. Here, we used a random seed process, placing a seed in the Ionian Sea to simulate a TLC under similar atmospheric and oceanographic conditions of medicane Ianos. Subsequently, the anomalies generated by medicane Ianos in the Ionian Sea were applied to the PMIP4-CMIP6 variables of SST, air temperature at 1000 hPa, MSLP and specific humidity at 1000 hPa, in order to simulate a TLC under LIG conditions. Outputs of the model provide the 3-hourly track of the TLC, along with values for the maximum wind speed (V_{max}).

The assessment of wind radii for each track point was performed using a modified Holland (1980) wind profile adapted for Mediterranean TLC (see Supplementary Material S3). The pressure deficit ΔP was taken relative to the standard pressure (Pn) of 1013.25 hPa, as in Ferrarin et al. (2023). The radius of maximum wind (R_{max}) was similarly estimated using a multi-method ensemble incorporating empirical ΔP–R_{max} relationships, wind-speed scaling, and theoretical Holland (1980) profile constraints, resulting in R_{max} values generally between 90 and 200 km for LIG-TLC.

Once V_{max} and R_{max} were known for each TLC track point, the radial pressure gradient (dp/dR) was assessed to forecast the $MSLP_{LIG}$ values using the Bernoulli relationship:

$$\frac{V_{max}^2}{R_{max}} = \frac{1}{\rho}\frac{dp}{dR} \quad \text{(Eq. 1)}$$

$$\frac{dp}{dR} = \rho\frac{V_{max}^2}{R_{max}} \quad \text{(Eq. 2)}$$

Where $\frac{dp}{dR}$ is the radial pressure gradient, and ρ is the air density, V_{max} is the maximum wind speed, R_{max} is the radius of maximum wind intensity. The percentage of increase in V_{max}^2 with respect to the baseline state corresponds to the same percentage of increase in the pressure gradient $\left(\%\frac{dp}{dR_{max}}\right)$, supposing R_{max} remains constant. Assuming a standard pressure P_n equal to 1013.25 hPa, and $V_{max,LIG}$ is a result from the model of Lin et al. (2023), the $MSLP_{LIG}$ values have been assessed in the following way:

$$\Delta P_{LIG} = \left(P_n - MSLP\right) \times \left(\frac{V_{max,LIG}}{V_{max}}\right)^2$$
$$MSLP_{LIG} = P_n - \Delta P_{LIG} \quad \text{(Eq. 3)}$$

$MSLP_{LIG}$, R_{max} and $V_{max,LIG}$ were inserted into the Delft3D Tropical Cyclone module (Delft3D-TC) to generate initial conditions for water level (WL) and significant wave height (SWH) at the regional scale. For this, we used a spatial domain with a grid resolution of 0.1° × 0.1°, interpolating bathymetric data from EMODnet. Then, a nested grid was built in southeastern Sicily with a resolution of 0.05 × 0.05°, in order to extract the boundary conditions for a local modeling (Supplementary Material S4). Coupled simulations have been performed by means of Delft3D-WAVE with Delft3D-FLOW to incorporate wave-current interaction(Lyddon et al., 2019; Whitham G.B., 1974). Delft3D-FLOW accounts for wave-current interactions via radiation stresses (based on Longuet-Higgins and Stewart (1964) and vortex forces (Martins et al., 2022). Wave effects, simulated by Delft3D-WAVE, are coupled iteratively with hydrodynamic processes, influencing currents via radiation stress gradients and wave-enhanced bottom shear stress. The bottom shear stress is computed using a quadratic friction law, with a Manning roughness coefficient of 0.07 (Pignatelli et al., 2010). A computational time step of 10 min was adopted to resolve water level and spectral SWH variations, for a time range equivalent to 16 September 2020 – 19 September 2020.

3.4. Modeling of earthquake-generated tsunami

The parameters for the F3-segment fault (Fig. 5) were used to simulate the initial sea surface displacement using elastic dislocation model of Okada, 1985. This model calculates the static deformation of the seafloor resulting from a sudden slip on a fault plane, which is subsequently translated into the initial condition for tsunami propagation. The Okada model provides a closed-form solution for the surface displacement (vertical, north, and east components) caused by a finite rectangular fault in an elastic, homogeneous, isotropic half-space. The required inputs are the fault geometry (strike, dip, rake, length, and width), the hypocentral location and depth, and the slip magnitude. For our simulation, the distributed slip of 4.8 m along the F3 fault plane was translated into a uniform slip model, generating the initial sea-surface dislocation pattern that serves as the tsunami source.

This initial water displacement field was then implemented as the forcing condition in the Delft3D-Tsunami and Delft3D-FLOW suite to model wave propagation. Delft3D-FLOW solves the non-linear shallow water equations, which are appropriate for long-wave phenomena like tsunamis, using an unstructured finite-volume grid that allows for high resolution in complex coastal areas. The tsunami simulation was

performed in two stages to balance computational efficiency and nearshore accuracy. First, propagation was simulated on a regional-scale coarse grid ($0.02^\circ \times 0.02^\circ$ of cell resolution) covering the Ionian Sea and southeastern Sicily to capture the basin-wide wave dynamics. The time series of water levels are made available at the boundaries of a nested local grid ($0.005^\circ \times 0.005^\circ$ of cell resolution). Second, these boundary conditions were used to drive a high-resolution local grid focused on the Capo Muro di Porco coastline, enabling detailed modelling of coastal flooding and wave flow at the boundary sites. The total simulation time was 15 min with a 1-min output interval, sufficient to capture the first and most energetic tsunami waves.

3.5. Morphodynamic models of extreme waves: hurricanes and tsunami

The evaluation of wave flow able to dislodge the coastal boulders of Capo Muro di Porco under LIG scenario was performed through XBeach model. The boundary conditions of XBeach model derived from outputs of forcing conditions obtained in the Delft3D simulations of TLC and tsunami scenarios. The XBeach model was run in surfbeat mode, which resolves short-wave group forcing on infragravity timescales, enabling the simulation of wave setup, run-up, and wave-driven coastal processes during extreme events. The spatial domain was created using a high-resolution grid generated with the Delft3D-GRID module, featuring an offshore cell resolution of 18×18 m and a nearshore cell resolution of 4×4 m (see Supplementary Material S4 for details on grid resolutions). LIG-LiDAR data were interpolated onto the grid to define the morpho-topography, while multibeam data from Scicchitano et al. (2016) were used to interpolate the nearshore and offshore areas.

4. Results

The flow needed to initiate boulder motion highlighted a scenario where CTBDs could be dislodged when the sea level was higher than present and compatible with the LIG scenario. The chronology of the marine terrace deposits (119 ka) suggests the boulder movements occurred during the LIG post-highstand regressive phase, rather than at the sea-level highstand (~125 ka). Furthermore, the extreme wave events would have been stronger than present, suggesting wave flow compatible with tsunami or intensified medicane during LIG.

4.1. Results-wave flow needed to initiate boulder motions

The field surveys performed in Capo Muro di Porco site revealed a strong relationship between boulder locations and coastal landforms atop of the cliff. The distribution of coastal boulders is patchy, reflecting the varying roughness of the rocky coastline. Notably, the Miocene paleodune surface, extending from the cliff edge to roughly 40 m inland, is completely devoid of boulders. This absence indicates that the paleodune likely served as a preferential pathway that facilitated boulder transport, a role enabled by its low surface roughness of 0.178 as measured by TLS. In contrast, the extensive marine deposit landward of the paleodune has a high roughness value of 0.5, which would have hindered the inland transport of boulders (Fig. 6a). Flow assessed from incipient motion formula range from 1.79 m/s to 7.55 m/s under subaerial/submerged conditions, and 3.96 m/s to 7.56 m/s under joint bounded conditions (Fig. 6b). Average flow velocities for each presetting condition resulted as follow:

- SB-sliding resulted equal to 3.1 ± 0.6 m/s;
- SB-overturning resulted equal to 4.7 ± 0.8 m/s;
- SB-saltation resulted equal to 5.8 ± 1.1 m/s;
- JB-saltation/lifting resulted equal to 5.84 ± 1.1 m/s.

4.2. Results – LIG extreme wave events at the regional scale

To achieve the best performance of the TLC during LIG, we applied

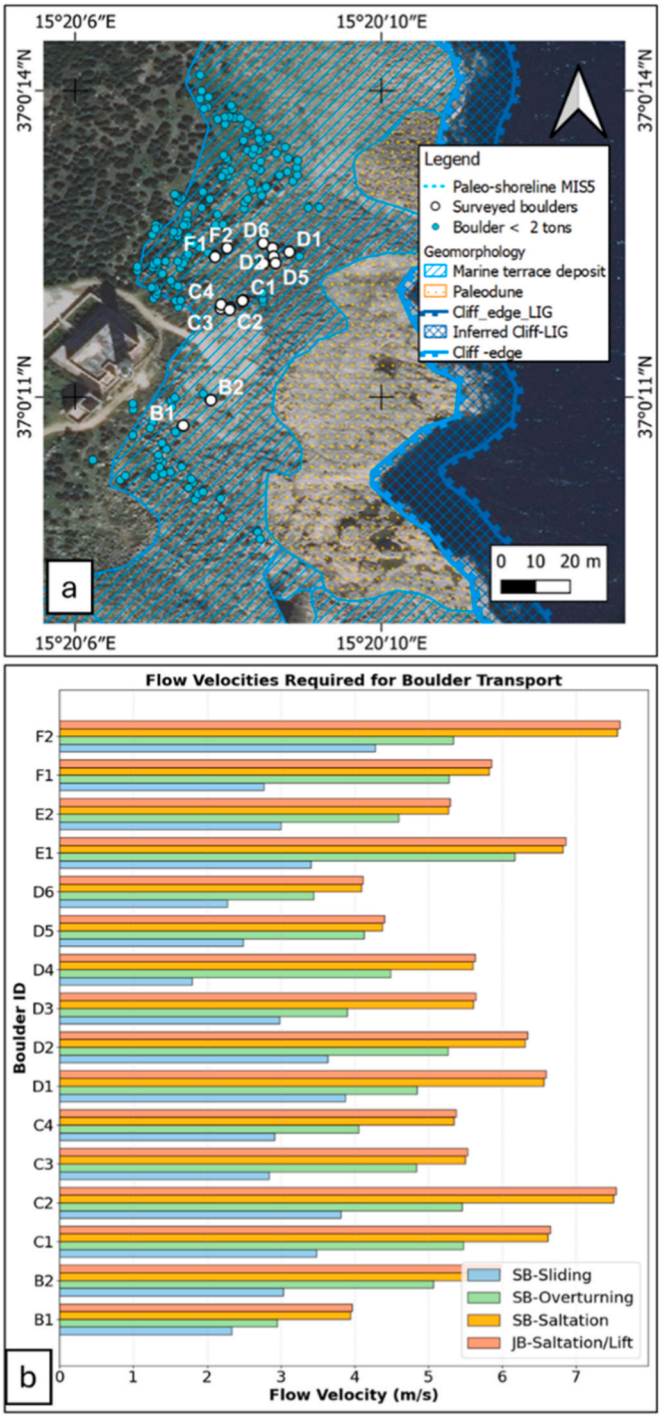

Fig. 6. – Geomorphological features reconstructed for the LIG scenario at Capo Muro di Porco; a) buffer area of ancient cliff indicated from Inferred Cliff-LIG polygon and location of coastal boulders surveyed through TLS; b) flows needed to initiate boulder motion, which were assessed through incipient motion formulas for Subaerial/Submerged (SB) and Joint Bounded (JB) conditions.

the Lin et al. (2023) model with ERA5 reanalysis variables for medicane Ianos (Fig. 7a and b). Subsequently, we applied the same model altering the atmospheric and oceanographic conditions with the anomalies reported in Table 3, which are computed against the ERA5 dataset period 1995-2025. The intensity variables revealed a TLC that was 24% more intense than the baseline scenario (Fig. 7c).

The cyclone intensity variables (V_{max} and MSLP) along the simulated

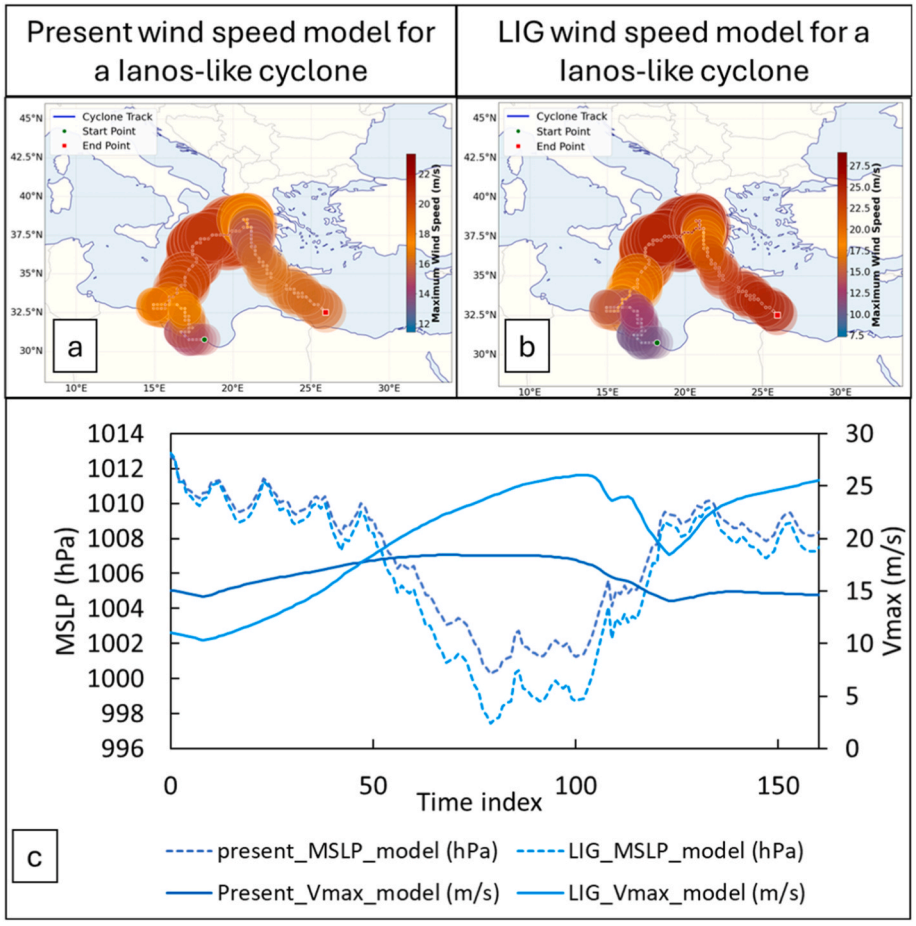

Fig. 7. – Cyclone intensity variables modelled according to Lin et al. (2023) model: a) wind speed and Rmax for medicane Ianos conditions using ERA5 atmospheric variables from 15 to 20 September 2020; b) wind speed and Rmax under LIG forcing scenarios derived by applying LIG anomalies to ERA5 data; c) maximum wind speed (Vmax) and MSLP minima along cyclone tracks for both present-day and LIG forcing scenarios.

Table 3
– Medicane Ianos-induced anomalies, computed from ERA5 data, were subsequently applied to PMIP4-CMIP6 variables (lig127k-month9).

Anomaly of sea surface temperature – ΔSST (°C)	Anomaly of air temperature at 1000 hPa – Δta (°C)	Anomaly of specific humidity – ΔQ (g/kg)	Anomaly of mean sea level pressure – ΔMSLP (hPa)
−3.42	−3.35	0.0002	1.2

tracks were used to force the regional Delft3D-TC model, incorporating the LIG topography at 119 ka. This corrected LIG sea level was a critical boundary condition for simulating coastal flooding and wave action during the LIG. Conversely, simulation with present sea level cannot determine flooding surface over the CTBD location (as already observed in Scicchitano et al., 2022).

Regional-scale modeling of the LIG cyclone indicates that the combined effect of stronger winds, lower central pressure, and higher sea level resulted in significantly increased significant wave heights (SWH) and water levels along the Ionian coast of Sicily compared to present-day conditions (Fig. 8a and b-c). The spatial pattern of maximum SWH shows a broad area of wave heights exceeding 8 m offshore of southeastern Sicily (Fig. 8d and e-f), with peak values focused on promontories such as Capo Muro di Porco site.

Similarly, the earthquake-generated tsunami scenario, modelled with the same corrected LIG sea level, produced a widespread wave field originating from the F3 fault segment on the Malta Escarpment. The simulated tsunami propagation (Fig. 8g–i) shows direct energy focusing toward the study area, with maximum offshore wave amplitudes exceeding 3 m.

4.3. *Results – wave flow from morphodynamic model and comparison with theoretical model*

The outputs from the regional models (water level and SWH time series) were then used as boundary conditions for the high-resolution XBeach morphodynamic model at Capo Muro di Porco site. The results of the local flooding simulations are summarized in Fig. 9, which shows the root-mean-square wave height (Hrms) at the Capo Muro di Porco coast for three scenarios: (a) present-day medicane Ianos forcing on LIG topography, (b) intensified LIG cyclone forcing on LIG topography, and (c) LIG tsunami forcing on LIG topography. All three scenarios generate flooding that inundates the boulder positions, but the spatial extent and magnitude of H_{rms} are greatest for the LIG cyclone (Fig. 9b) and tsunami scenario (Fig. 9 c).

In terms of wave flow velocity, a key parameter for boulder dislodgement, both the LIG cyclone and LIG tsunami scenarios produced velocities exceeding 3.1 m/s, surpassing the theoretical thresholds required for initiating sliding motion (see Section 4.1). The wave flows simulated with present sea level (displaced 13.6 m below LIG sea level in Fig. 10a) do not reach the elevation of CTBDs (both for medicane and tsunami scenarios). The present-day cyclone scenario, even on LIG topography, generated lower flow velocities, insufficient to mobilize the largest boulders (Fig. 10b). Only the wave flow generated by the LIG tsunami was powerful enough to displace CTBDs through all transport modes (sliding, overturning, and saltation).

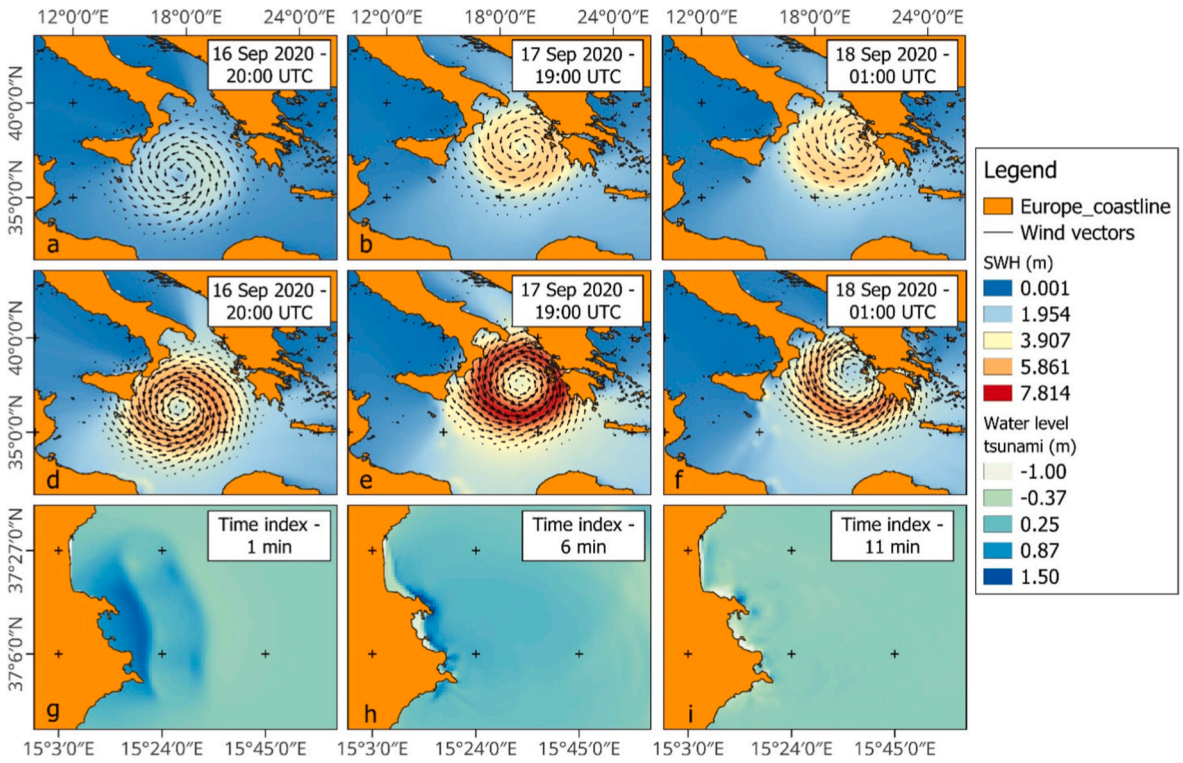

Fig. 8. Regional modelling outputs for extreme wave scenarios during the LIG: a-b-c) SWH and surface wind vectors simulated for the current forcings of medicane Ianos; d-e-f) SWH and wind vectors simulated for the intensified cyclone under LIG conditions; g-h-i) tsunami water surface elevation at selected time steps (1, 6, and 11 min after fault rupture), simulated for a Mw 7.4 earthquake on the F3 segment of the Malta Escarpment. All simulations incorporate corrected LIG sea level (119 ka).

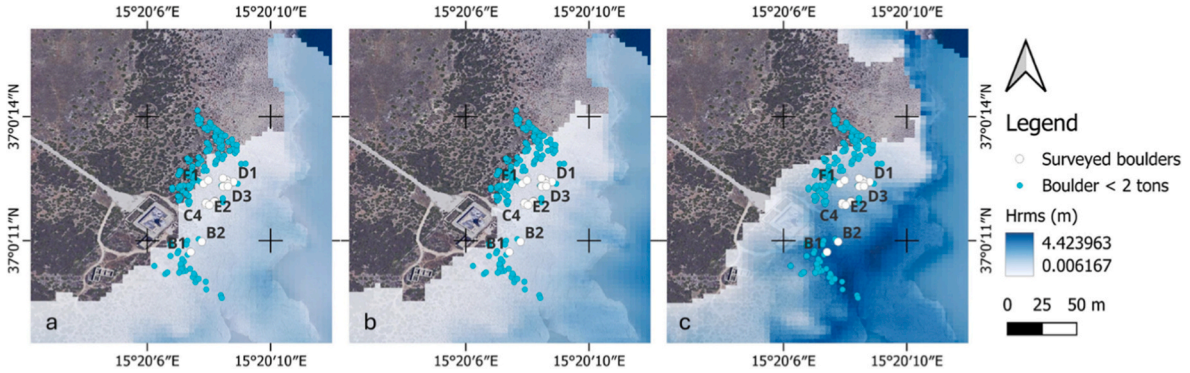

Fig. 9. – Coastal flooding modelled through XBeach for LIG scenarios: a) Hrms modelled using present-day medicane conditions over LIG topography; b) Hrms modelled using intensified cyclone conditions over LIG topography; c) Hrms modelled using tsunami conditions over LIG topography.

5. Discussion

The elevated RSL during MIS 5e is recognized globally, with estimates placing the mean sea level during the LIG highstand between 6 and 9 m higher than today (Dutton and Lambeck, 2012; Kopp et al., 2009). In the Mediterranean basin, tectonically stable regions usually display boulder deposits at elevations ranging from 6 to 7 m, as observed on the northwestern coast of Egypt (Hegab and El-Asmar, 1995) and along rocky coasts of Apulia (Italy) (Delle Rose, 2024; Delle Rose et al., 2020; Mastronuzzi and Pignatelli, 2012; Mastronuzzi and Sansò, 2004; Scardino et al., 2020). The attribution of coastal boulders to a specific LIG scenario is strongly constrained by the resolution of RSL curves. In this work, we used the average values from the Grant et al. (2014) sea-level curve for MIS 5e, which has an associated uncertainty of approximately 12 m under 95% of confidence (see Fig. 4). To better constrain the RSL attribution, the direct evidence of sea-level indicators has been considered. In the study area of Capo Muro di Porco, the presence of an inner edge of MIS5e located at 22-27 m of elevation suggested a significant contribution from local uplift -estimated at 0.16 mm/a (Meschis et al., 2020), and 0.12 mm/a of GIA rate in southeastern Sicily (Stocchi et al., 2018). This required elevation directly engages the long-standing scientific controversy surrounding whether the LIG was characterized by "superstorms" of unprecedented intensity(Hearty, 1997; Hearty et al., 2002). Studies of massive boulders located on North Eleuthera Island, Bahamas, initially suggested that storms of greater intensity than those in the Holocene were necessary for their emplacement during the LIG (Bourgeois and Weiss, 2009; Hearty, 1997; Hearty et al., 2002; Kindler and Strasser, 2000). However, more recent hydrodynamic modelling in the Bahamas proposed an alternative interpretation, arguing that storms of historical intensity (such as Hurricane

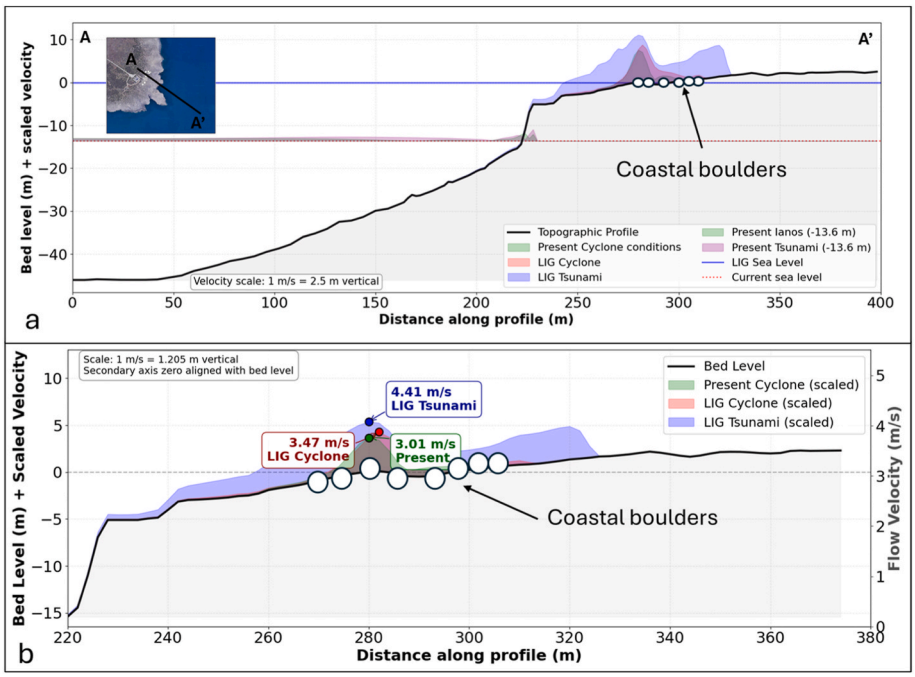

Fig. 10. – Wave flow profiles from XBeach modelling: a) LIG bed level displaying scaled velocities relative to LIG sea level (blue reference) and current sea level (red reference, ~13.6 m below corrected LIG sea level); b) analysis of LIG wave flow scenarios with maximum scaled velocities for various wave impact types. (For interpretation of the references to colour in this figure legend, the reader is referred to the Web version of this article.)

Sandy) were sufficient to transport these boulders if combined with the high LIG RSL (RSL from +3.5 m to +12.5 m) (Rovere et al., 2017). Similarly, analysis of an MIS 5e boulder ridge in Sal Island, Cape Verde, showed that, while present-day waves could not reach the feature, the transport threshold for boulders (sliding and overturning) was exceeded only when RSL exceeded +5m(Rovere et al., 2026). The results align with this framework, demonstrating that the presence of LIG RSL was the necessary condition for extreme wave events to be effective.

However, considering the CTBD masses and their distance from the cliff-edge (up to 105 m), it could be reasonable that multiple transport mechanisms occurred in Capo Muro di Porco. Based on the outcomes of theoretical flow values and XBeach model results, the CTBDs could have been mobilized by either an intensified cyclonic event (under a LIG warmer climate) or an earthquake-generated tsunami (energy equivalent to 1693 AD tsunami event). Both scenarios produced cliff overtopping and flow velocities exceeding the empirical thresholds (3.1 m/s) when coupled with the LIG RSL. The ratio between the theoretical flow of the incipient motion formula and modelled flow through XBeach is shown in Fig. 11 for each pre-setting condition under LIG scenarios.

The LIG cyclone scenario is supported by paleoclimate modelling, which suggests that the Mediterranean basin experienced significantly higher storm surge extremes during the regressive phase of LIG, particularly in the summer (Scussolini et al., 2023). These extreme events correlate strongly with anomalies in seasonal sea level pressure minima and are likely linked to the warmer SSTs prevailing in the Mediterranean during the LIG (Hoffman et al., 2017). Despite Lin et al.,

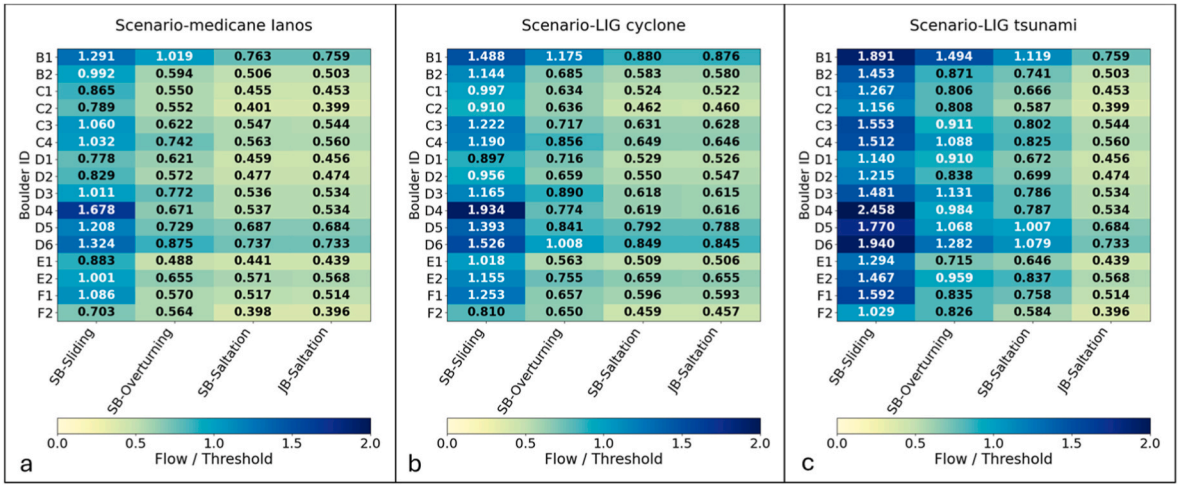

Fig. 11. Heatmaps illustrating the relative wave-induced flow intensity experienced by each boulder under different extreme wave impacts, across four transport modes: sliding, overturning, saltation (for submerged or subaerial isolated boulders in pre-transport settings), and saltation/lifting (for joint-bounded boulders in pre-transport settings). Each cell represents the ratio of the maximum flow velocity at the boulder location to the empirical threshold flow velocity required to initiate transport for the respective mode; a) medicane Ianos scenario with LIG paleotopography; b) Intensified cyclone scenario under LIG atmospheric and oceanographic conditions; c) Tsunami scenario with LIG paleotopography.

2023 model constraints that limit maximum medicane intensities to approximately 45 m/s (see Supplementary Material S3)—consistent with realistic medicane—our simulations still demonstrate a 24% intensification under LIG conditions. This suggests that even with conservative modelling assumptions, warmer sea surface temperatures during the LIG would have substantially increased medicane potential intensity.

The alternative mechanism involved simulating a significant earthquake (Mw 7.4) along the active F3 segment of the MESC, comparable to the earthquake-generated tsunami of 1693 AD (Scicchitano et al., 2022). This simulation successfully generated the required wave flows when the LIG RSL was incorporated as a boundary condition. On the other hand, earthquake-generated tsunami initiated transport under a wider range of pre-transport conditions, enabling sliding, overturning, and saltation movements in both subaerial and submerged scenarios (Fig. 11c). For the Capo Muro di Porco, the integration of high-resolution mapping (Fig. 6a and supplementary Material S4) revealed crucial geomorphological controls on CTBD dislodgments. The Miocene paleodune, characterized by a notably low roughness value (0.178), likely served as a preferential pathway enabling landward boulder displacement. This contrasts sharply with the area's extensive marine terraced deposits, which exhibit a higher roughness (0.5) and would have effectively hindered further inland transport. On the other hand, the spatial assessment of the roughness values was essential for the parametrization of XBeach morphodynamic model. The paleodune surfaces are characterized by higher wave flow compared to the surrounding marine terrace surfaces, which in turn hinder boulder transport. This behaviour has been confirmed by model output, revealing a peak in wave velocity near the cliff edge for each modelled scenario (Fig. 10).

The difficulty in definitively distinguishing between storm and tsunami origins remains a global methodological hurdle for CTBDs (Bryant and Nott, 2001; Cox et al., 2020), as evidenced by MIS 5e boulder deposits in New Zealand tentatively attributed to a tsunami 2-3 m high (Kennedy et al., 2007). The climatic conditions of the LIG serve as a robust process analogue for assessing future coastal hazards in a warming world. Modelling of LIG scenarios demonstrates that rising sea levels have the potential to significantly increase wave flows and associated wave energy. Furthermore, warmer sea temperatures during the LIG likely amplified tropical cyclone development mechanisms. Although LIG SST were only about 1.3 °C higher than pre-industrial levels, IPCC projections indicate that SST could rise by 3 to 5 °C above those levels in the coming centuries (IPCC et al., 2021; 2019). The projected future SST warming under the SSP2-4.5 scenario (3.1 °C of centennial warming) exceeds the SST warming observed during the LIG (1.8 °C of centennial warming, Obreht et al. (2022);IPCC et al., 2019). This greater warming would enhance intense medicane development in a near future, leading to more intense cyclones (González-Alemán et al., 2019, 2023; Koseki et al., 2021).

6. Conclusions

Based on the comprehensive analysis and modelling results presented in this study, the CTBDs at Capo Muro di Porco (south-eastern Sicily) represent a significant geological archive of extreme wave events during the LIG post-highstand regressive phase. By integrating high-resolution morpho-topographic surveys, hydrodynamic modelling, and paleoenvironmental reconstructions, this research demonstrates that the mobilization of these large boulders—positioned atop a 10-m-high cliff beyond the reach of modern storms and tsunamis—can be satisfactorily explained only under LIG conditions. CTBDS at Capo Muro di Porco do not necessarily record Holocene extreme events. Instead, their emplacement may be preferentially associated with non-Holocene conditions, particularly periods characterised by elevated relative sea level, such as the LIG regressive phase. Key findings indicate that the RSL during the LIG regressive phase, estimated at about 13.65 m above present one in the Capo Muro di Porco, was a critical prerequisite for extreme waves to reach the CTBD locations. Numerical simulations of both intensified TLC and tsunami scenarios under reconstructed LIG paleotopography highlighted that wave flow velocities exceeded the theoretical thresholds required to initiate boulder motion (sliding, overturning, and saltation). Specifically, the modelled LIG cyclone, intensified by warmer sea surface temperatures and altered atmospheric conditions, and a potential Mw 7.4 earthquake-generated tsunami from the F3 fault segment, both produced sufficient wave flows (>3.1 m/s in sliding movement) to dislodge and transport the boulders.

The study also highlights the importance of local geomorphological controls, such as the low-roughness Miocene paleodune surface, which likely acted as a preferential pathway for boulder transport inland. This detailed reconstruction moves beyond the traditional storm-versus-tsunami debate by showing that either mechanism could have been effective under the combined influence of higher RSL and, in the case of storms, a warmer, more energetic LIG climate. These results contribute to the broader discussion by demonstrating that LIG CTBDs do not necessarily require “superstorms” of unprecedented intensity for their emplacement. Instead, they underscore the amplifying role of RSL—a condition that transformed regional wave hydrodynamics and extended the inundation footprint of extreme events.

From this perspective, the apparent rarity of CTBDs along Mediterranean rocky coasts does not necessarily reflect the infrequency of extreme wave events, but rather the limited occurrence of favourable boundary conditions required for their formation and preservation. Consequently, previously reported Mediterranean CTBDs lacking robust chronological constraints may warrant re-evaluation, as their emplacement could plausibly predate the Holocene and be linked to earlier high-sea-level intervals. These findings highlight the need for integrated geomorphological, hydrodynamic, and chronological approaches when interpreting CTBDs in semi-enclosed basins. More broadly, they underscore the importance of considering sea-level-controlled boundary conditions when using extreme coastal deposits to reconstruct past wave climates and assess future coastal hazards under ongoing sea-level rise. As a process analogue for future warming, this work implies that contemporary sea-level rise, coupled with projected increases in tropical cyclone intensity, may significantly enhance coastal hazard potentials in the Mediterranean and other similar regions. Thus, the boulders of Capo Muro di Porco serve not only as a fingerprint of past extreme waves but also as a tangible warning of the heightened vulnerability of coastal systems in a warmer world.

Author contributions

Conceptualization: Giovanni Scardino, Giovanni Scicchitano.

Data curation: Giovanni Scardino, Alok Kushabaha.

Formal analysis: Giovanni Scicchitano, Alessio Rovere, Mario Marcello Miglietta.

Funding acquisition: Giovanni Scicchitano, Giovanni Scardino.

Investigation: Giovanni Scicchitano, Giovanni Scardino.

Methodology: Giovanni Scicchitano, Giovanni Scardino, Mario Marcello Miglietta, NAK Nandasena.

Project administration: Giovanni Scicchitano.

Resources: Giovanni Scicchitano.

Software: Giovanni Scardino, Alok Kushabaha, Marco Anzidei, Tommaso Alberti.

Supervision: Giovanni Scicchitano.

Validation: Giovanni Scardino, Mario Marcello Miglietta, Alessio Rovere, Tommaso Alberti, NAK Nandasena.

Visualization: Marco Anzidei, Tommaso Alberti, NAK Nandasena, Alessio Rovere.

Writing – original draft: Giovanni Scardino.

Writing – review and editing: Mario Marcello Miglietta, Marco Anzidei, Tommaso Alberti, NAK Nandasena, Alessio Rovere, Giovanni Scicchitano.

Financial support

This research has been funded by the PRIN 2022 PNRR project titled "ARCHIMEDE – Multidisciplinary approach to better define vulnerability and hazard of Medicanes along the Ionian coasts of Sicily" (CUP H53D23011380001, Principal Investigator Giovanni Scicchitano).

Declaration of competing interest

The authors declare that they have no known competing financial interests or personal relationships that could have appeared to influence the work reported in this paper.

Acknowledgements

This work has greatly benefited from contributions of the ERC SEED UNIBA project "Get aHead Of the MEdicanes: strategies for the COASTal environment – HOMECOAST" (Principal Investigator Dr. Giovanni Scardino, PhD). Giovanni Scardino and Tommaso Alberti received funding from Ministero dell'Università e della Ricerca under the call Fondo Italiano per la Scienza 2022-2023 (FIS-2) for the project "Mediterranean Extreme Events and Tipping elements in a changing climate on multiple spatiotemporal scales", grant number FIS-2023-00159, CUP: D53C240005450001 (Principal Investigator Dr. Tommaso Alberti, PhD). This paper and related research have been conducted within the framework of the Italian inter-university PhD course in sustainable development and climate change (link: https://www.phd-sdc.it/, last access: 1 July 2025) "Medichange" (responsible Prof. Giovanni Scicchitano, PhD). Data analyses presented in this work were supported by the Marine Science Laboratory of the Department of Earth and Geo-environmental Sciences at the University of Bari Aldo Moro (Responsible: Prof. Giovanni Scicchitano, PhD).

Alessio Rovere acknowledges funding from the European Research Council (ERG) under the European Union's Horizon 2020 research and innovation programme (grant agreement No. 802414). Views and opinions expressed are however those of the author(s) only and do not necessarily reflect those of the European Union or the European Research Council Executive Agency. Neither the European Union nor the granting authority can be held responsible for them.

Appendix A. Supplementary data

Supplementary data to this article can be found online at https://doi.org/10.1016/j.quascirev.2026.110012.

Data availability

All data and/or code is contained within the submission.

References

Amies, J.D., Rohling, E.J., Grant, K.M., Rodríguez-Sanz, L., Marino, G., 2019. Quantification of African monsoon runoff during last interglacial sapropel S5. Paleoceanogr. Paleoclimatol. 34, 1487–1516. https://doi.org/10.1029/2019PA003652.

Antonioli, F., Kershaw, S., Renda, P., Rust, D., Belluomini, G., Cerasoli, M., Radtke, U., Silenzi, S., 2006. Elevation of the last interglacial highstand in sicily (Italy): a benchmark of coastal tectonics. Quaternary International, Quaternary sea-level changes: contributions from the 32nd IGC 145–146, 3–18. https://doi.org/10.1016/j.quaint.2005.07.002.

Anzidei, M., Scicchitano, G., Scardino, G., Bignami, C., Tolomei, C., Vecchio, A., Serpelloni, E., De Santis, V., Monaco, C., Milella, M., Piscitelli, A., Mastronuzzi, G., 2021. Relative sea-level rise scenario for 2100 along the Coast of South Eastern Sicily (Italy) by InSAR data, satellite images and high-resolution topography. Remote Sens. 13, 1108. https://doi.org/10.3390/rs13061108.

Argnani, A., Armigliato, A., Pagnoni, G., Zaniboni, F., Tinti, S., Bonazzi, C., 2012. Active tectonics along the submarine slope of south-eastern Sicily and the source of the 11 January 1693 earthquake and tsunami. Nat. Hazards Earth Syst. Sci. 12, 1311–1319. https://doi.org/10.5194/nhess-12-1311-2012.

Argnani, A., Bonazzi, C., 2005. Malta escarpment fault zone offshore eastern Sicily: pliocene-quaternary tectonic evolution based on new multichannel seismic data. Tectonics 24. https://doi.org/10.1029/2004TC001656.

Autret, R., Didier, D., Suanez, S., Stéphan, P., Ammann, J., Baudry, J., Erlingsson, B., Sigurðarson, S., 2023. Cliff-top boulder morphodynamics on the high–energy volcanic rocky coast of the Reykjanes Peninsula (SW Iceland). Mar. Geol. 456, 106984. https://doi.org/10.1016/j.margeo.2022.106984.

Autret, R., Dodet, G., Fichaut, B., Suanez, S., Leckler, F., Ardhuin, F., Grandjean, P., Allemand, P., Filipot, J.-F., Amman, J., David, L., 2016. A comprehensive hydro-geomorphic study of cliff-top storm deposits on Banneg Island during winter 2013–2014. Mar. Geol. 382. https://doi.org/10.1016/j.margeo.2016.09.014.

Autret, R., Dodet, G., Suanez, S., Roudaut, G., Fichaut, B., 2017. Long–term variability of supratidal coastal Boulder activation in Brittany (France). Geomorphology 304. https://doi.org/10.1016/j.geomorph.2017.12.028.

Azzaro, R., Barbano, M.S., 2000. Analysis of the seismicity of Southeastern Sicily: a proposed tectonic interpretation. Ann. Geophys. 43. https://doi.org/10.4401/ag-3628.

Bianca, M., Monaco, C., Tortorici, L., Cernobori, L., 1999. Quaternary normal faulting in southeastern Sicily (Italy):a seismic source for the 1693 large earthquake. Geophys. J. Int. 139, 370–394. https://doi.org/10.1046/j.1365-246x.1999.00942.x.

Billi, A., Minelli, L., Orecchio, B., Presti, D., 2009. Runup distribution for the 1908 Messina tsunami in Italy: observed data versus expected curves. Bulletin of The Seismological Society of America - BULL SEISMOL SOC AMER 99, 3502–3509. https://doi.org/10.1785/0120090128.

Biolchi, S., Furlani, S., Antonioli, F., Baldassini, N., Causon Deguara, J., Devoto, S., Di Stefano, A., Evans, J., Gambin, T., Gauci, R., Mastronuzzi, G., Monaco, C., Scicchitano, G., 2016. Boulder accumulations related to extreme wave events on the eastern coast of Malta. Nat. Hazards Earth Syst. Sci. 16, 737–756. https://doi.org/10.5194/nhess-16-737-2016.

Bourgeois, J., Weiss, R., 2009. "Chevrons" are not mega-tsunami deposits—A sedimentologic assessment. Geology 37 (1), 403–406. https://doi.org/10.1130/G25246A.

Bourrouilh-Le Jan, F.G., Talandier, J., 1985. Sedimentation et fracturation de haute energie en milieu recifal: Tsunamis, ouragans et cyclones et leurs effets sur la sedimentologie et la geomorphologie d'un atoll: Motu et hoa, a rangiroa, Tuamotu, Pacifique SE. Mar. Geol. 67, 263–333. https://doi.org/10.1016/0025-3227(85)90095-7.

Braitenberg, C., Mariani, P., Tunini, L., Grillo, B., Nagy, I., 2011. Vertical crustal motions from differential tide gauge observations and satellite altimetry in southern Italy. J. Geodyn. 51, 233–244. https://doi.org/10.1016/j.jog.2010.09.003.

Bryant, E.A., Nott, J., 2001. Geological indicators of large tsunami in Australia. Nat. Hazards 24, 231–249. https://doi.org/10.1023/A:1012034021063.

Canavesio, R., Cohen, O., Pons-Branchu, E., Costa, S., 2023. Atoll islets reshaping processes induced by extreme cyclonic waves and calm weather. Evidence from two centuries of megablocks emergences and coral rubble displacements in Anaa, Rangiroa and Tikehau atolls (western Tuamotu archipelago - french Polynesia). Mar. Geol. 464, 107140. https://doi.org/10.1016/j.margeo.2023.107140.

Cane, T., Rohling, E.J., Kemp, A.E.S., Cooke, S., Pearce, R.B., 2002. High-resolution stratigraphic framework for Mediterranean sapropel S5: defining temporal relationships between records of eemian climate variability. Palaeogeogr. Palaeoclimatol. Palaeoecol. 183, 87–101. https://doi.org/10.1016/S0031-0182(01)00461-8.

Causon Deguara, J., Gauci, R., 2017. Evidence of extreme wave events from boulder deposits on the south-east coast of Malta (Central Mediterranean). Nat. Hazards 86. https://doi.org/10.1007/s11069-016-2525-4.

Causon-Deguara, J., Gauci, R., Inkpen, R., 2025. Coastal boulder deposits in the Mediterranean: a comprehensive review of research and findings. Med. Geosc. Rev. 7, 255–274. https://doi.org/10.1007/s42990-025-00164-8.

Corradino, M., Faraci, C., Monaco, C., Pepe, F., 2025. Coastal boulder production controlled by columnar joints of ignimbrite and extreme waves: insights from the high-energy coast of Pantelleria Island (Sicily Channel, Mediterranean Sea). Nat. Hazards 121, 3621–3655. https://doi.org/10.1007/s11069-024-06936-z.

Cosentino, D., Gliozzi, E., 1992. Considerazioni sulle velocita' di sollevamento di depositi eutirreniani dell'Italia meridionale e della Sicilia. Memor. Soc. Geol. Ital. 42, 653–665.

Cox, R., 2020. Megagravel deposits on the west coast of Ireland show the impacts of severe storms. Weather 75, 72–77. https://doi.org/10.1002/wea.3677.

Cox, R., Ardhuin, F., Dias, F., Autret, R., Beisiegel, N., Earlie, C.S., Herterich, J.G., Kennedy, A., Paris, R., Raby, A., Schmitt, P., Weiss, R., 2020. Systematic review shows that work done by storm waves can be misinterpreted as tsunami-related because commonly used hydrodynamic equations are flawed. Front. Mar. Sci. 7. https://doi.org/10.3389/fmars.2020.00004.

Cox, R., Bourke, M.C., Engel, M., Kennedy, A.B., Lau, A., Suanez, S., Boulton, S.J., Oliveira, M.A., Paris, R., Salmanidou, D., Spiske, M., Stephenson, W., Roberts, S., Switzer, A.D., Mhammdi, N., Cullen, N.D., Watanabe, M., 2025. Understanding extreme-wave hazards on high-energy coasts requires a standardised approach to field data collection: analysis and recommendations. Nat. Hazards Earth Syst. Sci. 25, 4203–4226. https://doi.org/10.5194/nhess-25-4203-2025.

Cox, R., Jahn, K.L., Watkins, O.G., Cox, P., 2018. Extraordinary boulder transport by storm waves (west of Ireland, winter 2013–2014), and criteria for analysing coastal boulder deposits. Earth Sci. Rev. 177, 623–636. https://doi.org/10.1016/j.earscirev.2017.12.014.

Cox, R., O'Boyle, L., Cytrynbaum, J., 2019. Imbricated Coastal Boulder deposits are formed by storm waves, and can preserve a long-term storminess record. Sci. Rep. 9, 10784. https://doi.org/10.1038/s41598-019-47254-w.

Cultrera, F., Barreca, G., Scarfì, L., Monaco, C., 2015. Fault reactivation by stress pattern reorganization in the Hyblean foreland domain of SE Sicily (Italy) and seismotectonic implications. Tectonophysics 661, 215–228. https://doi.org/10.1016/j.tecto.2015.08.043.

Davtian, N., Ménot, G., Fagault, Y., Bard, E., 2019. Western Mediterranean Sea paleothermometry over the last glacial cycle based on the novel RI-OH index. Paleoceanogr. Paleoclimatol. 34, 616–634. https://doi.org/10.1029/2018PA003452.

Delle Rose, M., 2024. Annual Coastal Boulder mobility detected in 2017–2021 remote sensing imagery and its relation to marine storms (Gulf of Taranto, Mediterranean Sea). Geosciences 14, 136. https://doi.org/10.3390/geosciences14050136.

Delle Rose, M., Fidelibus, C., Martano, P., Orlanducci, L., 2020. Storm-induced boulder displacements: inferences from field surveys and hydrodynamic equations. Geosciences 10, 1–21. https://doi.org/10.3390/geosciences10090374.

Dewey, J.F., Ryan, P.D., 2017. Storm, rogue wave, or tsunami origin for megaclast deposits in western Ireland and North Island, New Zealand? Proc. Natl. Acad. Sci. USA 114, E10639–E10647. https://doi.org/10.1073/pnas.1713233114.

Dixit, Y., Toucanne, S., Fontanier, C., Pasquier, V., Lora, J.M., Jouet, G., Tripati, A., 2020. Enhanced western mediterranean rainfall during past interglacials driven by North Atlantic pressure changes. Quat. Int. 553, 1–13. https://doi.org/10.1016/j.quaint.2020.08.017.

Dunán-Avila, P., Authemayou, C., Jaud, M., Pedoja, K., Jara-Muñoz, J., Bertín, S., Peñalver-Hernández, L., Floc'h, F., Nuñez-Labañino, A., Winckler, P., Pierre-Toledo, J., de Jesus Benítez-Frometa, P., Ross-Cabrera, H., Letortu, P., Rodríguez-Valdés, A.R., Coutín-Lobaina, N., Chauveau, D., 2024. Geomorphological signatures of known hurricanes and validation of theoretical emplacement formulations: coastal boulder deposits on Cuban low-lying marine terraces. Mar. Geol., 107438 https://doi.org/10.1016/j.margeo.2024.107438.

Dutton, A., Scicchitano, G., Monaco, C., Desmarchelier, J.M., Antonioli, F., Lambeck, K., Esat, T.M., Fifield, L.K., McCulloch, M.T., Mortimer, G., 2009. Uplift rates defined by U-series and 14C ages of serpulid-encrusted speleothems from submerged caves near Siracusa, Sicily (Italy). Quat. Geochronol. 4, 2–10. https://doi.org/10.1016/j.quageo.2008.06.003.

Dutton, A., Lambeck, K., 2012. Ice volume and Sea level during the last interglacial. Science 337, 216–219. https://doi.org/10.1126/science.1205749.

Emanuel, Kerry, Alberti, Tommaso, Bourdin, Stella, Camargo, Suzana J., Faranda, Davide, et al., 2025. CYCLOPs: a unified framework for surface flux-driven cyclones outside the tropics. Weather Clim. Dyn. 6 (3), 901–926. https://doi.org/10.5194/wcd-6-901-2025. https://wcd.copernicus.org/articles/6/901/2025/. (Accessed 5 September 2025).

Engel, M., Pupo, F.M., Ortega, Z.H., Brill, D., 2025. Massive boulders shifted along the coast of Guantánamo, Cuba, during Hurricane Matthew (2016). Erdkunde 79, 191–210. https://doi.org/10.3112/erdkunde.2025.03.02.

Etienne, S., Paris, R., 2010. Boulder accumulations related to storms on the south coast of the Reykjanes Peninsula (Iceland). Geomorphology, Rock Coast Geomorphology 114, 55–70. https://doi.org/10.1016/j.geomorph.2009.02.008.

Eyring, V., Cox, P.M., Flato, G.M., Gleckler, P.J., Abramowitz, G., Caldwell, P., Collins, W.D., Gier, B.K., Hall, A.D., Hoffman, F.M., Hurtt, G.C., Jahn, A., Jones, C.D., Klein, S.A., Krasting, J.P., Kwiatkowski, L., Lorenz, R., Maloney, E., Meehl, G.A., Pendergrass, A.G., Pincus, R., Ruane, A.C., Russell, J.L., Sanderson, B.M., Santer, B. D., Sherwood, S.C., Simpson, I.R., Stouffer, R.J., Williamson, M.S., 2019. Taking climate model evaluation to the next level. Nature Clim Change 9, 102–110. https://doi.org/10.1038/s41558-018-0355-y.

Ferranti, L., Antonioli, F., Anzidei, M., Monaco, C., Stocchi, P., 2010. The timescale and spatial extent of vertical tectonic motions in Italy: insights from relative sea-level changes studies. J. Virtual Explor. 36. https://doi.org/10.3809/jvirtex.2009.00255.

Ferranti, L., Antonioli, F., Mauz, B., Amorosi, A., Dai Pra, G., Mastronuzzi, G., Monaco, C., Orrù, P., Pappalardo, M., Radtke, U., Renda, P., Romano, P., Sansò, P., Verrubbi, V., 2006. Markers of the last interglacial sea-level high stand along the coast of Italy: tectonic implications. Quaternary International, Quaternary sea-level changes: contributions from the 32nd IGC 145–146, 30–54. https://doi.org/10.1016/j.quaint.2005.07.009.

Ferrarin, C., Pantillon, F., Davolio, S., Bajo, M., Miglietta, M.M., Avolio, E., Carrió, D.S., Pytharoulis, I., Sanchez, C., Patlakas, P., González-Alemán, J.J., Flaounas, E., 2023. Assessing the coastal hazard of Medicane Ianos through ensemble modelling. Nat. Hazards Earth Syst. Sci. 23, 2273–2287. https://doi.org/10.5194/nhess-23-2273-2023.

Fichaut, B., Suanez, S., 2011. Quarrying, transport and deposition of cliff-top storm deposits during extreme events: banneg Island, Brittany. Marine Geology, Special Issue on Boulders as a signature of storms on rock coasts 283, 36–55. https://doi.org/10.1016/j.margeo.2010.11.003.

Furlani, S., Cucchi, F., 2013. Downwearing rates of vertical limestone surfaces in the intertidal zone (Gulf of Trieste, Italy). Mar. Geol. 343, 92–98. https://doi.org/10.1016/j.margeo.2013.06.005.

Gambino, S., Barreca, G., Gross, F., Monaco, C., Gutscher, M.-A., Alsop, G.I., 2022. Assessing the rate of crustal extension by 2D sequential restoration analysis: a case study from the active portion of the Malta Escarpment. Basin Res. 34, 321–341. https://doi.org/10.1111/bre.12621.

Gambino, S., Barreca, G., Gross, F., Monaco, C., Krastel, S., Gutscher, M.-A., 2021. Deformation pattern of the northern sector of the Malta Escarpment (offshore SE-Sicily, Italy); fault dimension, slip prediction and seismotectonic implications. Front. Earth Sci. 8. https://doi.org/10.3389/feart.2020.594176.

Gao, G., Colin, C., Liu, Z., Plautre, A., Wu, J., Sabatier, P., Sepulcre, S., Siani, G., Pinna, R., Dapoigny, A., 2025. Dynamics of the North African climate over the last 600 kyr based on mineralogical and geochemical investigations of deep sediments in the western Mediterranean Sea. Global Planet. Change 255, 105131. https://doi.org/10.1016/j.gloplacha.2025.105131.

González-Alemán, J.J., Insua-Costa, D., Bazile, E., González-Herrero, S., Miglietta, M.M., Groenemeijer, P., Donat, M.G., 2023. Anthropogenic warming had a crucial role in triggering the historic and destructive Mediterranean Derecho in summer 2022. Bull. Am. Meteorol. Soc. 104, E1526–E1532. https://doi.org/10.1175/BAMS-D-23-0119.1.

González-Alemán, J.J., Pascale, S., Gutierrez-Fernandez, J., Murakami, H., Gaertner, M. A., Vecchi, G.A., 2019. Potential increase in hazard from Mediterranean hurricane activity with global warming. Geophys. Res. Lett. 46, 1754–1764. https://doi.org/10.1029/2018GL081253.

Goto, K., Miyagi, K., Kawamata, H., Imamura, F., 2010. Discrimination of boulders deposited by tsunamis and storm waves at Ishigaki Island, Japan. Mar. Geol. 269, 34–45. https://doi.org/10.1016/j.margeo.2009.12.004.

Grant, K.M., Grimm, R., Mikolajewicz, U., Marino, G., Ziegler, M., Rohling, E.J., 2016. The timing of Mediterranean sapropel deposition relative to insolation, sea-level and African monsoon changes. Quat. Sci. Rev. 140, 125–141. https://doi.org/10.1016/j.quascirev.2016.03.026.

Grant, K.M., Rohling, E.J., Ramsey, C.B., Cheng, H., Edwards, R.L., Florindo, F., Heslop, D., Marra, F., Roberts, A.P., Tamisiea, M.E., Williams, F., 2014. Sea-level variability over five glacial cycles. Nat. Commun. 5, 5076. https://doi.org/10.1038/ncomms6076.

Grasso, M., Lentini, F., 1982. Sedimentary and tectonic evolution of the eastern Hyblean Plateau (southeastern Sicily) during late Cretaceous to Quaternary time. Palaeogeogr. Palaeoclimatol. Palaeoecol. 39, 261–280. https://doi.org/10.1016/0031-0182(82)90025-6.

Grezio, A., Anzidei, M., Baglione, E., Brizuela, B., Di Manna, P., Selva, J., Taroni, M., Tonini, R., Vecchio, A., 2024. Including sea-level rise and vertical land movements in probabilistic tsunami hazard assessment for the Mediterranean Sea. Sci. Rep. 14, 28873. https://doi.org/10.1038/s41598-024-79770-9.

Hall, A., Hansom, J., Williams, D., Jarvis, J., 2006. Distribution, geomorphology and lithofacies of cliff-top storm deposits: examples from the high-energy coasts of Scotland and Ireland. Mar. Geol. 232, 131–155. https://doi.org/10.1016/j.margeo.2006.06.008.

Hansen, J., Sato, M., Hearty, P., Ruedy, R., Kelley, M., Masson-Delmotte, V., Russell, G., Tselioudis, G., Cao, J., Rignot, E., Velicogna, I., Tormey, B., Donovan, B., Kandiano, E., von Schuckmann, K., Kharecha, P., Legrande, A.N., Bauer, M., Lo, K.-W., 2016. Ice melt, sea level rise and superstorms: evidence from paleoclimate data, climate modeling, and modern observations that 2 °C global warming could be dangerous. Atmos. Chem. Phys. 16, 3761–3812. https://doi.org/10.5194/acp-16-3761-2016.

Hansom, J., Hall, A., 2009. Magnitude and frequency of extra-tropical North Atlantic cyclones. Quat. Int. 195, 42–52. https://doi.org/10.1016/j.quaint.2007.11.010.

Hayes, C.T., Martínez-García, A., Hasenfratz, A.P., Jaccard, S.L., Hodell, D.A., Sigman, D. M., Haug, G.H., Anderson, R.F., 2014. A stagnation event in the deep South Atlantic during the last interglacial period. Science 346, 1514–1517. https://doi.org/10.1126/science.1256620.

Hearty, P.J., 1997. Boulder deposits from large waves during the last interglaciation on North Eleuthera Island, Bahamas. Quat. Res. 48, 326–338. https://doi.org/10.1006/qres.1997.1926.

Hearty, P.J., Hollin, J.T., Neumann, A.C., O'Leary, M.J., McCulloch, M., 2007. Global sea-level fluctuations during the last Interglaciation (MIS 5e). Quat. Sci. Rev. 26, 2090–2112. https://doi.org/10.1016/j.quascirev.2007.06.019.

Hearty, P.J., Tormey, B.R., Neumann, A.C., 2002. Discussion of "Palaeoclimatic significance of co-occurring wind- and water-induced sedimentary structures in the last-interglacial coastal deposits from Bermuda and the Bahamas" (Kindler and Strasser, 2000, Sedimentary Geology, 131, 1–7). Sediment. Geol. 147, 429–435. https://doi.org/10.1016/S0037-0738(01)00142-7.

Hearty, P.J., Tormey, B.R., 2017. Sea-level change and superstorms; geologic evidence from the last interglacial (MIS 5e) in The Bahamas and Bermuda offers ominous prospects for a warming Earth. Mar. Geol. 390, 347–365. https://doi.org/10.1016/j.margeo.2017.05.009.

Hegab, O.A., El-Asmar, H.M., 1995. Last interglacial stratigraphy in the burg El-Arab region of the northwestern coast of Egypt. Quat. Int. 29–30, 23–30. https://doi.org/10.1016/1040-6182(95)00004-3.

Henriquet, M., Dominguez, S., Barreca, G., Malavieille, J., Cadio, C., Monaco, C., 2019. Deep origin of the dome-shaped hyblean Plateau, Southeastern sicily: a new tectono-magmatic model. Tectonics 38, 4488–4515. https://doi.org/10.1029/2019TC005548.

Henriquet, M., Peyret, M., Dominguez, S., Barreca, G., Malavieille, J., Monaco, C., 2021. Pseudo-3D Ground Deformation Map of Sicily Derived from Sentinel-1 InSAR time-series EGU21-7105.

Hersbach, Hans, Bell, Bill, Berrisford, Paul, Hirahara, Shoji, Horányi, András, et al., 2020. The ERA5 global reanalysis. Quart. J. R. Meteorol. Soc. 146 (730), 1999–2049. https://doi.org/10.1002/qj.3803. https://rmets.onlinelibrary.wiley.com/doi/10.1002/qj.3803. (Accessed 15 June 2020).

Heslop, D., Amarathunga, U., Rohling, E.J., 2023. Estimating Plio-Pleistocene north African monsoon runoff into the Mediterranean Sea and temperature impacts. Paleoceanogr. Paleoclimatol. 38. https://doi.org/10.1029/2023PA004677 e2023PA004677.

Hoffman, J.S., Clark, P.U., Parnell, A.C., He, F., 2017. Regional and global sea-surface temperatures during the last interglaciation. Science 355, 276–279. https://doi.org/10.1126/science.aai8464.

Holland, G., 1980. An analytic model of the wind and pressure profiles in hurricanes. Mon. Weather Rev. 108, 1212–1218.

Huan, D., Yan, Q., Wei, T., 2023. Unfavorable environmental conditions for tropical cyclone genesis over the western North Pacific during the Last Interglacial based on PMIP4 simulations. Atmospheric and Oceanic Science Letters, Special Issue: Climate Variability, Climate Prediction and Climate Extremes - to commemorate the 20th Anniversary of Nansen-Zhu International Research Centre 16, 100395. https://doi.org/10.1016/j.aosl.2023.100395.

Huang, X., Yang, S., Haywood, A., Jiang, D., Wang, Y., Sun, M., Tang, Z., Ding, Z., 2021. Warming-induced northwestward migration of the Asian summer monsoon in the geological past: evidence from climate simulations and geological reconstructions. J. Geophys. Res. Atmos. 126. https://doi.org/10.1029/2021JD035190.

Incarbona, A., Marino, G., Di Stefano, E., Grelaud, M., Pelosi, N., Rodríguez-Sanz, L., Rohling, E.J., 2022. Middle-late Pleistocene Eastern Mediterranean nutricline depth and coccolith preservation linked to Monsoon activity and Atlantic Meridional Overturning Circulation. Global Planet. Change 217, 103946. https://doi.org/10.1016/j.gloplacha.2022.103946.

Inghilesi, R., Corsini, S., Guiducci, F., Arseni, A., 2000. Statistical analysis of extreme waves on the Italian coasts from 1989 to 1999. Boll. Geofis. Teor. Appl. 41, 315–337.

IPCC, 2019. In: Pörtner, [H.-O., Roberts, D.C., Masson-Delmotte, V., Zhai, P., Tignor, M., Poloczanska, E., Mintenbeck, K., Alegría, A., Nicolai, M., Okem, A., Petzold, J., Rama, B., Weyer, N.M. (Eds.), Special Report on the Ocean and Cryosphere in a Changing Climate, p. 765. Working Group II Technical Support Unit.

IPCC, 2021. Summary for policymakers. In: Masson-Delmotte, V., Zhai, P., Pirani, A., Connors, S.L., Péan, C., Berger, S., Caud, N., Chen, Y., Goldfarb, L., Gomis, M.I., Huang, M., Leitzell, K., Lonnoy, E., Matthews, J.B.R., Maycock, T.K., Waterfield, T., Yelekçi, O., Yu, R., Zhou, B. (Eds.), Climate Change 2021: the Physical Science Basis. Contribution of Working Group I to the Sixth Assessment Report of the Intergovernmental Panel on Climate Change. Cambridge University Press, p. 3949.

Kageyama, M., Braconnot, P., Harrison, S.P., Haywood, A.M., Jungclaus, J., Otto-Bliesner, B.L., Peterschmitt, J.-Y., Abe-Ouchi, A., Albani, S., Bartlein, P.J., Brierley, C., Crucifix, M., Dolan, A., Fernandez-Donado, L., Fischer, H., Hopcroft, P. O., Ivanovic, R.F., Lambert, F., Lunt, D.J., Mahowald, N.M., Peltier, W.R., Phipps, S. J., Roche, D.M., Schmidt, G.A., Tarasov, L., Valdes, P.J., Zhang, Q., Zhou, T., 2016. PMIP4-CMIP6: the contribution of the Paleoclimate Modelling Intercomparison Project to CMIP6. Geosci. Model Dev. Discuss. (GMDD) 11, 1033–1057.

Kageyama, M., Sime, L.C., Sicard, M., Guarino, M.-V., de Vernal, A., Stein, R., Schroeder, D., Malmierca-Vallet, I., Abe-Ouchi, A., Bitz, C., Braconnot, P., Brady, E. C., Cao, J., Chamberlain, M.A., Feltham, D., Guo, C., LeGrande, A.N., Lohmann, G., Meissner, K.J., Menviel, L., Morozova, P., Nisancioglu, K.H., Otto-Bliesner, B.L., O'ishi, R., Ramos Buarque, S., Salas y Melia, D., Sherriff-Tadano, S., Stroeve, J., Shi, X., Sun, B., Tomas, R.A., Volodin, E., Yeung, N.K.H., Zhang, Q., Zhang, Z., Zheng, W., Ziehn, T., 2021. A multi-model CMIP6-PMIP4 study of Arctic sea ice at 127 ka: sea ice data compilation and model differences. Clim. Past 17, 37–62. https://doi.org/10.5194/cp-17-37-2021.

Kallel, N., Duplessy, J.-C., Labeyrie, L., Fontugne, M., Paterne, M., 2004. Mediterranean Sea palaeohydrology and pluvial periods during the late Quaternary. In: Battarbee, R.W., Gasse, F., Stickley, C.E. (Eds.), Past Climate Variability Through Europe and Africa. Springer, Netherlands, Dordrecht, pp. 307–324. https://doi.org/10.1007/978-1-4020-2121-3_15.

Kennedy, A., Cox, R., Engel, M., Speyrer, E., Lau, A., Mori, N., 2025. The inundation signatures on rocky coastlines global database for coastal boulder deposits (ISROC-DB). Mar. Geol. 487, 107581. https://doi.org/10.1016/j.margeo.2025.107581.

Kennedy, A.B., Cox, R., Dias, F., 2021. Storm waves may be the source of some "Tsunami" coastal Boulder deposits. Geophys. Res. Lett. 48. https://doi.org/10.1029/2020GL090775 e2020GL090775.

Kennedy, D.M., Tannock, K.L., Crozier, M.J., Rieser, U., 2007. Boulders of MIS 5 age deposited by a tsunami on the coast of Otago, New Zealand. Sedimentary Geology, Sedimentary Features of Tsunami Deposits - Their Origin, Recognition and Discrimination: An Introduction 200, 222–231. https://doi.org/10.1016/j.sedgeo.2007.01.005.

Köhler, M., Lau, A., Nakata, K., Goto, K., Goff, J., Köhler, D., Penisoni, M., 2025. Discovery of the world's largest cliff-top boulder: initial insights and numerical simulation of its transport on a 30–40 m high cliff on Tongatapu (Tonga). Mar. Geol. 487, 107567. https://doi.org/10.1016/j.margeo.2025.107567.

Kindler, P., Strasser, A., 2000. Palaeoclimatic significance of co-occurring wind- and water-induced sedimentary structures in the last-interglacial coastal deposits from Bermuda and the Bahamas. Sediment. Geol. 131, 1–7. https://doi.org/10.1016/S0037-0738(99)00123-2.

Kopp, R.E., Simons, F.J., Mitrovica, J.X., Maloof, A.C., Oppenheimer, M., 2009. Probabilistic assessment of sea level during the last interglacial stage. Nature 462, 863–867. https://doi.org/10.1038/nature08686.

Korbar, T., Navratil, D., Denamiel, C., Kordić, B., Biolchi, S., Vilibić, I., Furlani, S., 2022. Coarse-clast storm deposit and solitary boulders on the Island of Mana (NP Kornati, central adriatic, Croatia). Geosciences 12, 355. https://doi.org/10.3390/geosciences12100355.

Kortekaas, S., Dawson, A.G., 2007. Distinguishing tsunami and storm deposits: an example from Martinhal, SW Portugal. Sedimentary Geology, Sedimentary Features of Tsunami Deposits - Their Origin, Recognition and Discrimination: An Introduction 200, 208–221. https://doi.org/10.1016/j.sedgeo.2007.01.004.

Koseki, S., Mooney, P., Cabos Narvaez, W.D., Gaertner, M., de la Vara, A., González-Alemán, J., 2021. Modelling a tropical-like cyclone in the Mediterranean Sea under present and warmer climate. Nat. Hazards Earth Syst. Sci. 21, 53–71. https://doi.org/10.5194/nhess-21-53-2021.

Kushabaha, A., Scardino, G., Sabato, G., Miglietta, M.M., Flaounas, E., Monforte, P., Marsico, A., De Santis, V., Borzì, A.M., Scicchitano, G., 2024. ARCHIMEDE—An innovative Web-GIS platform for the study of medicanes. Remote Sens. 16, 2552. https://doi.org/10.3390/rs16142552.

Lambeck, K., Anzidei, M., Antonioli, F., Benini, A., Esposito, A., 2004. Sea level in Roman time in the Central Mediterranean and implications for recent change. Earth Planet Sci. Lett. 224, 563–575. https://doi.org/10.1016/j.epsl.2004.05.031.

Lang, N., Wolff, E.W., 2011. Interglacial and glacial variability from the last 800 ka in marine, ice and terrestrial archives. Clim. Past 7, 361–380. https://doi.org/10.5194/cp-7-361-2011.

Levy, E.J., Vonhof, H.B., Bar-Matthews, M., Martínez-García, A., Ayalon, A., Matthews, A., Silverman, V., Raveh-Rubin, S., Zilberman, T., Yasur, G., Schmitt, M., Haug, G.H., 2023. Weakened AMOC related to cooling and atmospheric circulation shifts in the last interglacial Eastern Mediterranean. Nat. Commun. 14, 5180. https://doi.org/10.1038/s41467-023-40880-z.

Lin, J., Rousseau-Rizzi, R., Lee, C.-Y., Sobel, A., 2023. An open-source, physics-based, tropical cyclone downscaling model with intensity-dependent steering. J. Adv. Model. Earth Syst. 15. https://doi.org/10.1029/2023MS003686 e2023MS003686.

Longuet-Higgins, M.S., Stewart, R.w., 1964. Radiation stresses in water waves; a physical discussion, with applications. Deep Sea Res. A 11, 529–562. https://doi.org/10.1016/0011-7471(64)90001-4.

Lyddon, C.E., Brown, J.M., Leonardi, N., Saulter, A., Plater, A.J., 2019. Quantification of the uncertainty in coastal storm hazard predictions due to wave-current interaction and wind forcing. Geophys. Res. Lett. 46, 14576–14585. https://doi.org/10.1029/2019GL086123.

Maouche, S., Morhange, C., Meghraoui, M., 2009. Large boulder accumulation on the Algerian coast evidence tsunami events in the western Mediterranean. Mar. Geol. 262, 96–104.

Marino, G., 2008. Palaeoceanography of the Interglacial Eastern Mediterranean Sea.

Marino, G., Rohling, E.J., Rijpstra, W.I.C., Sangiorgi, F., Schouten, S., Damsté, J.S.S., 2007. Aegean Sea as driver of hydrographic and ecological changes in the eastern Mediterranean. Geology 35, 675–678. https://doi.org/10.1130/G23831A.1.

Marino, G., Rohling, E.J., Rodríguez-Sanz, L., Grant, K.M., Heslop, D., Roberts, A.P., Stanford, J.D., Yu, J., 2015. Bipolar seesaw control on last interglacial sea level. Nature 522, 197–201. https://doi.org/10.1038/nature14499.

Marriner, Nick, Kaniewski, David, Morhange, Christophe, Flaux, Clément, Giaime, Matthieu, et al., 2017. Tsunamis in the geological record: Making waves with a cautionary tale from the Mediterranean. Sci. Adv. 3 (10), e1700485. https://doi.org/10.1126/sciadv.1700485. https://www.science.org/doi/10.1126/sciadv.1700485.

Martins, K., Bertin, X., Mengual, B., Pezerat, M., Lavaud, L., Guérin, T., Zhang, Y.J., 2022. Wave-induced mean currents and setup over barred and steep sandy beaches. Ocean Model. 179, 102110. https://doi.org/10.1016/j.ocemod.2022.102110.

Martrat, B., Grimalt, J.O., Lopez-Martinez, C., Cacho, I., Sierro, F.J., Flores, J.A., Zahn, R., Canals, M., Curtis, J.H., Hodell, D.A., 2004. Abrupt temperature changes in the Western mediterranean over the past 250,000 years. Science 306, 1762–1765. https://doi.org/10.1126/science.1101706.

Martrat, B., Jimenez-Amat, P., Zahn, R., Grimalt, J.O., 2014. Similarities and dissimilarities between the last two deglaciations and interglaciations in the North Atlantic region. Quat. Sci. Rev. 99, 122–134. https://doi.org/10.1016/j.quascirev.2014.06.016.

Mastronuzzi, G., Pignatelli, C., 2012. The boulder berm of Punta Saguerra (Taranto, Italy): a morphological imprint of the Rossano Calabro tsunami of April 24, 1836? Earth Planets Space 64, 829–842. https://doi.org/10.5047/eps.2011.08.018.

Mastronuzzi, G., Sansò, P., 2004. Large boulder accumulations by extreme waves along the Adriatic coast of southern Apulia (Italy). Quat. Int. 120, 173–184. https://doi.org/10.1016/j.quaint.2004.01.016.

Maxwell, K., Westphal, H., Rovere, A., 2021. A standardized database of Last Interglacial (MIS 5e) sea-level indicators in Southeast Asia. https://doi.org/10.5194/essd-13-4313-2021.

McDonagh, Bethany, Clementi, Emanuela, Goglio, Anna Chiara, Pinardi, Nadia, 2024. The characteristics of tides and their effects on the general circulation of the Mediterranean Sea. Ocean Sci. 20 (4), 1051–1066. https://doi.org/10.5194/os-20-1051-2024. https://os.copernicus.org/articles/20/1051/2024/. (Accessed 29 August 2024).

Meschis, M., Scicchitano, G., Roberts, G.P., Robertson, J., Barreca, G., Monaco, C., Spampinato, C., Sahy, D., Antonioli, F., Mildon, Z.K., Scardino, G., 2020. Regional deformation and offshore crustal local faulting as combined processes to explain uplift through time constrained by investigating differentially uplifted late Quaternary paleoshorelines: the Foreland hyblean Plateau, SE sicily. Tectonics 39. https://doi.org/10.1029/2020TC006187 e2020TC006187.

Miglietta, M.M., Flaounas, E., González-Alemán, J.J., Panegrossi, G., Gaertner, M.A., Pantillon, F., Pasquero, C., Schultz, D.M., D'Adderio, L.P., Dafis, S., Husson, R., Ricchi, A., Carrió, D.S.C., Davolio, S., Fita, L., Picornell, M.Á., Pytharoulis, I., Raveh-Rubin, S., Scoccimarro, E., Bernini, L., Cavicchia, L., Conte, D., Ferretti, R., Flocas, H., Gutiérrez-Fernández, J., Hatzaki, M., Santaner, V.H., Jansà, A., Patlakas, P., 2025. Defining medicanes: bridging the knowledge gap between tropical and extratropical cyclones in the Mediterranean. Bull. Am. Meteorol. Soc. 106, E1955–E1971. https://doi.org/10.1175/BAMS-D-24-0289.1.

Minamidate, K., Goto, K., 2024. Unveiling the history and nature of paleostorms in the Holocene. Earth Sci. Rev. 253, 104774. https://doi.org/10.1016/j.earscirev.2024.104774.

Monaco, C., Bianca, M., Catalano, S., Guidi, G., Tortorici, L., 2002. Sudden change in the Late Quaternary tectonic regime in eastern Sicily: evidences from geological and geomorphological features. Bollettino- Societa Geologica Italiana SI 1, 901–913.

Nadia Mhammdi, F.M., Kelletat, D., M'Fedal Ahmamou, L.A., 2008. LARGE BOULDERS ALONG THE RABAT COAST (MOROCCO); POSSIBLE EMPLACEMENT BY THE NOVEMBER, 1st, 1755 A.D. TSUNAMI. Science of Tsunami Hazards.

Nandasena, N.A.K., Scicchitano, G., Scardino, G., Milella, M., Piscitelli, A., Mastronuzzi, G., 2022. Boulder displacements along rocky coasts: a new

deterministic and theoretical approach to improve incipient motion formulas. Geomorphology 407, 108217. https://doi.org/10.1016/j.geomorph.2022.108217.
Noormets, R., Crook, K.A.W., Felton, E.A., 2004. Sedimentology of rocky shorelines: 3.: hydrodynamics of megaclast emplacement and transport on a shore platform, Oahu, Hawaii. Sediment. Geol. 172, 41–65. https://doi.org/10.1016/j.sedgeo.2004.07.006.
Obreht, I., De Vleeschouwer, D., Wörmer, L., Kucera, M., Varma, D., Prange, M., Laepple, T., Wendt, J., Nandini-Weiss, S.D., Schulz, H., Hinrichs, K.-U., 2022. Last interglacial decadal sea surface temperature variability in the eastern Mediterranean. Nat. Geosci. 15, 812–818. https://doi.org/10.1038/s41561-022-01016-y.
Obreht, I., Wörmer, L., Varma, D., De Vleeschouwer, D., Schulz, H., Kucera, M., Hinrichs, K.-U., 2025. Influence of Mediterranean oceanographic and environmental conditions on molecular proxy-based Sea surface temperature reconstructions during the last interglacial. Paleoceanogr. Paleoclimatol. 40. https://doi.org/10.1029/2024PA004951 e2024PA004951.
O'ishi, R., Chan, W.-L., Abe-Ouchi, A., Sherriff-Tadano, S., Ohgaito, R., Yoshimori, M., 2021. PMIP4/CMIP6 last interglacial simulations using three different versions of MIROC: importance of vegetation. Clim. Past 17, 21–36. https://doi.org/10.5194/cp-17-21-2021.
Okada, Y., 1985. Surface deformation to shear and tensile faults in a halfspace. Bull. Seismol. Soc. Am. 75.
Osborne, A.H., Vance, D., Rohling, E.J., Barton, N., Rogerson, M., Fello, N., 2008. A humid corridor across the Sahara for the migration of early modern humans out of Africa 120,000 years ago. Proc. Natl. Acad. Sci. 105, 16444–16447. https://doi.org/10.1073/pnas.0804472105.
Otto-Bliesner, B.L., Braconnot, P., Harrison, S.P., Lunt, D.J., Abe-Ouchi, A., Albani, S., Bartlein, P.J., Capron, E., Carlson, A.E., Dutton, A., Fischer, H., Goelzer, H., Govin, A., Haywood, A., Joos, F., LeGrande, A.N., Lipscomb, W.H., Lohmann, G., Mahowald, N., Nehrbass-Ahles, C., Pausata, F.S.R., Peterschmitt, J.-Y., Phipps, S.J., Renssen, H., Zhang, Q., 2017. The PMIP4 contribution to CMIP6 – part 2: two interglacials, scientific objective and experimental design for Holocene and Last Interglacial simulations. Geosci. Model Dev. (GMD) 10, 3979–4003. https://doi.org/10.5194/gmd-10-3979-2017.
Otto-Bliesner, B.L., Brady, E.C., Tomas, R.A., Albani, S., Bartlein, P.J., Mahowald, N.M., Shafer, S.L., Kluzek, E., Lawrence, P.J., Leguy, G., Rothstein, M., Sommers, A.N., 2020. A comparison of the CMIP6 midHolocene and lig127k simulations in CESM2. Paleoceanogr. Paleoclimatol. 35. https://doi.org/10.1029/2020PA003957 e2020PA003957.
Otto-Bliesner, B.L., Rosenbloom, N., Stone, E.J., McKay, N.P., Lunt, D.J., Brady, E.C., Overpeck, J.T., 2013. How warm was the last interglacial? New model–data comparisons. Philos. Trans. R. Soc. A Math. Phys. Eng. Sci. 371, 20130097. https://doi.org/10.1098/rsta.2013.0097.
Pavlis, N.K., Holmes, S.A., Kenyon, S.C., Factor, J.K., 2012. The development and evaluation of the Earth Gravitational Model 2008 (EGM2008). J. Geophys. Res. Solid Earth 117. https://doi.org/10.1029/2011JB008916.
Pedoja, K., Dunán-Avila, P., Jara-Muñoz, J., Authemayou, C., Nuñez-Labañino, A., de Gelder, G., Chauveau, D., Peñalver, L., Frometa, P.D.J.B., Martin-Izquierdo, D., Abella, E.C., Bertin, S., Rodríguez-Valdés, Á.R., Arango-Arias, E.D., Traoré, K., Regard, V., 2023. On a 210 t Caribbean coastal boulder: the huracanolito seaward of the ruins of the Bucanero resort, Juragua, Oriente, Cuba. Earth Surf. Process. Landf. 48, 3074–3090. https://doi.org/10.1002/esp.5682.
Piatanesi, A., Tinti, S., 1998. A revision of the 1693 eastern Sicily earthquake and tsunami. J. Geophys. Res. Solid Earth 103, 2749–2758. https://doi.org/10.1029/97JB03403.
Pignatelli, C., Piscitelli, A., Damato, B., Mastronuzzi, G., 2010. Estimation of the value of manning's coefficient using terrestrial laser scanner techniques for the assessment of flooding by extreme waves. Zeitschrift fur Geomorphologie 54, 317–336. https://doi.org/10.1127/0372-8854/2010/0054S3-0030.
Pinardi, Nadia, Zavatarelli, Marco, Adani, Mario, Coppini, Giovanni, Fratianni, Claudia, et al., 2015. Mediterranean Sea large-scale low-frequency ocean variability and water mass formation rates from 1987 to 2007: A retrospective analysis. Prog. Oceanogr. 132, 318–332. https://doi.org/10.1016/j.pocean.2013.11.003. https://linkinghub.elsevier.com/retrieve/pii/S007966111300222X.
Rohling, E.J., Cane, T.R., Cooke, S., Sprovieri, M., Bouloubassi, I., Emeis, K.C., Schiebel, R., Kroon, D., Jorissen, F.J., Lorre, A., Kemp, A.E.S., 2002. African monsoon variability during the previous interglacial maximum. Earth Planet Sci. Lett. 202, 61–75. https://doi.org/10.1016/S0012-821X(02)00775-6.
Rohling, E.J., Hopmans, E.C., Sinninghe Damsté, J.S., 2006. Water column dynamics during the last interglacial anoxic event in the Mediterranean (Sapropel S5). Paleoceanography 21. https://doi.org/10.1029/2005PA001237.
Rohling, E.J., Sprovieri, M., Cane, T., Casford, J.S.L., Cooke, S., Bouloubassi, I., Emeis, K. C., Schiebel, R., Rogerson, M., Hayes, A., Jorissen, F.J., Kroon, D., 2004. Reconstructing past planktic foraminiferal habitats using stable isotope data: a case history for Mediterranean sapropel S5. Mar. Micropaleontol. 50, 89–123. https://doi.org/10.1016/S0377-8398(03)00068-9.
Roig-Munar, F.X., Rodríguez-Perea, A., Vilaplana, J.M., Martín-Prieto, J.A., Gelabert, B., 2019. Tsunami boulders in Majorca Island (Balearic Islands, Spain). Geomorphology 334, 76–90. https://doi.org/10.1016/j.geomorph.2019.02.012.
Rovere, A., Casella, E., Harris, D.L., Lorscheid, T., Nandasena, N.A.K., Dyer, B., Sandstrom, M.R., Stocchi, P., D'Andrea, W.J., Raymo, M.E., 2017. Giant boulders and Last Interglacial storm intensity in the North Atlantic. Proceedings of the National Academy of Sciences of the United States of America 114, 12144–12149. https://doi.org/10.1073/pnas.1712433114.
Rovere, A., Scicchitano, G., Casella, E., Scardino, G., Barile, C., Vieira, G., Nandasena, N. A.K., Ryan, D.D., Scussolini, P., Ramalho, R.S., 2026. Paleo extreme storm waves in the North Atlantic: geological evidence from Sal Island, Cape Verde Archipelago. Geomorphology 493, 110076. https://doi.org/10.1016/j.geomorph.2025.110076.
Rovida, A., Locati, M., Camassi, R., Lolli, B., Gasperini, P., 2020. The Italian earthquake catalogue CPTI15. Bull. Earthq. Eng. 18, 2953–2984. https://doi.org/10.1007/s10518-020-00818-y.
Rovida, A., Locati, M., Camassi, R., Lolli, B., Gasperini, P., Antonucci, A., 2022. Italian Parametric Earthquake Catalogue (CPTI15), Version 4.0. Istituto Nazionale di Geofisica e Vulcanologia (INGV). https://doi.org/10.13127/CPTI/CPTI15.4.
Ruban, Dmitry A., 2019. Coastal boulder deposits of the Neogene world: A synopsis. J. Mar. Sci. Eng. 7 (12), 446. https://doi.org/10.3390/jmse7120446. https://www.mdpi.com/2077-1312/7/12/446. (Accessed 5 December 2019).
Scardino, G., Piscitelli, A., Milella, M., Sansò, P., Mastronuzzi, G., 2020. Tsunami fingerprints along the Mediterranean coasts. Rend. Fis. Acc. Lincei 31, 319–335. https://doi.org/10.1007/s12210-020-00895-w.
Scardino, G., Rizzo, A., De Santis, V., Kyriakoudi, D., Rovere, A., Vacchi, M., Torrisi, S., Scicchitano, G., 2022a. Insights on the origin of multiple tsunami events affected the archaeological site of Ognina (south-eastern Sicily, Italy). Quaternary International, Lost Landscapes: Reconstructing the Evolution of Coastal Areas since the Late Pleistocene 638–639, 122–139. https://doi.org/10.1016/j.quaint.2021.09.013.
Scardino, G., Rovere, A., Barile, C., Nandasena, N.A.K., Chauveau, D., Dahm, M., Boyden, P., Bejarano, S., Casella, E., Kelly, H., Mijts, E., Scicchitano, G., 2025. Coastal boulders emplaced by extreme wave events impacting the ABC islands (Aruba, Bonaire, Curaçao; Leeward Antilles, Caribbean). Quat. Sci. Rev. 349, 109136. https://doi.org/10.1016/j.quascirev.2024.109136.
Scardino, G., Scicchitano, G., Chirivì, M., Costa, P.J.M., Luparelli, A., Mastronuzzi, G., 2022b. Convolutional neural network and optical flow for the assessment of wave and tide parameters from video analysis (LEUCOTEA): an innovative tool for coastal monitoring. Remote Sens. 14, 2994. https://doi.org/10.3390/rs14132994.
Schär, C., Frei, C., Lüthi, D., Davies, H., 1996. Surrogate climate-change scenarios for regional climate models. Geophysical Research Letters - GEOPHYS RES LETT 23, 669–672. https://doi.org/10.1029/96GL00265.
Scicchitano, G., Antonioli, F., Berlinghieri, E.F.C., Dutton, A., Monaco, C., 2008. Submerged archaeological sites along the Ionian coast of southeastern Sicily (Italy) and implications for the Holocene relative sea-level change. Quat. Res. 70, 26–39. https://doi.org/10.1016/j.yqres.2008.03.008.
Scicchitano, G., Berlinghieri, E.F.C., Antonioli, F., Spampinato, C.R., Monaco, C., 2016. Sacred landscapes and changing Sea levels: new interdisciplinary data from the early Neolithic to the present in South-Eastern sicily. In: Bailey, G.N., Harff, J., Sakellariou, D. (Eds.), Under the Sea: Archaeology and Palaeolandscapes of the Continental Shelf, Coastal Research Library. Springer International Publishing, Cham, pp. 233–253. https://doi.org/10.1007/978-3-319-53160-1_16.
Scicchitano, G., Costa, B., Di Stefano, A., Longhitano, S.G., Monaco, C., 2010. Tsunami and storm deposits preserved within a ria-type rocky coastal setting (Siracusa, SE Sicily). Zeitschrift für Geomorphologie, Supplementary Issues 54, 51–77. https://doi.org/10.1127/0372-8854/2010/0054S3-0019.
Scicchitano, G., Gambino, S., Scardino, G., Barreca, G., Gross, F., Mastronuzzi, G., Monaco, C., 2022. The enigmatic 1693 AD tsunami in the eastern Mediterranean Sea: new insights on the triggering mechanisms and propagation dynamics. Sci. Rep. 12, 9573. https://doi.org/10.1038/s41598-022-13538-x.
Scicchitano, G., Monaco, C., Tortorici, L., 2007. Large boulder deposits by tsunami waves along the Ionian coast of south-eastern Sicily (Italy). Mar. Geol. 238, 75–91. https://doi.org/10.1016/j.margeo.2006.12.005.
Scicchitano, G., Pignatelli, C., Spampinato, C.R., Piscitelli, A., Milella, M., Monaco, C., Mastronuzzi, G., 2012. Terrestrial Laser Scanner techniques in the assessment of tsunami impact on the Maddalena peninsula (south-eastern Sicily, Italy). Earth Planets Space 64, 889–903. https://doi.org/10.5047/eps.2011.11.009.
Scicchitano, G., Scardino, G., Tarascio, S., Monaco, C., Barracane, G., Locuratolo, G., Milella, M., Piscitelli, A., Mazza, G., Mastronuzzi, G., 2020. The first video witness of coastal Boulder displacements recorded during the impact of medicane "Zorbas" on Southeastern sicily. Water 12, 1497. https://doi.org/10.3390/w12051497.
Scicchitano, Giovanni, Scardino, Giovanni, Monaco, Carmelo, Piscitelli, Arcangelo, Milella, Maurilio, et al., 2021. Comparing impact effects of common storms and Medicanes along the coast of south-eastern Sicily. Mar. Geol. 439, 106556. https://doi.org/10.1016/j.margeo.2021.106556, 106556. https://linkinghub.elsevier.com/retrieve/pii/S0025322721001389.
Scicchitano, G., Monaco, C., 2006. Karstic caves and submerged paleo-shorelines in the coastal area between Capo Santa Panagia and Ognina (Siracusa, south-eastern Sicily). Alpine and Mediterranean Quaternary 19, 187–194.
Scussolini, P., Dullaart, J., Muis, S., Rovere, A., Bakker, P., Coumou, D., Renssen, H., Ward, P.J., Aerts, J.C.J.H., 2023. Modeled storm surge changes in a warmer world: the Last Interglacial. Clim. Past 19, 141–157. https://doi.org/10.5194/cp-19-141-2023.
Spampinato, C.R., Braitenberg, C., Monaco, C., Scicchitano, G., 2013. Analysis of vertical movements in eastern Sicily and southern Calabria (Italy) through geodetic leveling data. J. Geodyn. 66, 1–12. https://doi.org/10.1016/j.jog.2012.12.002.
Spampinato, C.R., Costa, B., Di Stefano, A., Monaco, C., Scicchitano, G., 2011. The contribution of tectonics to relative sea-level change during the Holocene in coastal south-eastern Sicily: new data from boreholes. Quaternary International, Tectonic Contribution to Relative Sea Level Change 232, 214–227. https://doi.org/10.1016/j.quaint.2010.06.025.
Spampinato, C.R., Scicchitano, G., Ferranti, L., Monaco, C., 2012. Raised Holocene paleo-shorelines along the Capo Schisò coast, Taormina: new evidence of recent co-seismic deformation in northeastern Sicily (Italy). J. Geodyn. 55, 18–31. https://doi.org/10.1016/j.jog.2011.11.007.
Stocchi, P., Vacchi, M., Lorscheid, T., de Boer, B., Simms, A.R., van de Wal, R.S.W., Vermeersen, B.L.A., Pappalardo, M., Rovere, A., 2018. MIS 5e relative sea-level

changes in the Mediterranean Sea: contribution of isostatic disequilibrium. Quat. Sci. Rev. 185, 122–134. https://doi.org/10.1016/j.quascirev.2018.01.004.

Suanez, S., Cox, R., André, G., Leballeur, L., Dodet, G., Ammann, J., Jaud, M., Mahéo, H., 2026. Long-term monitoring of coastal boulder deposits on Banneg Island: a good proxy for detection of extreme oceanic storms off West Brittany (France). Geomorphology 492, 110043. https://doi.org/10.1016/j.geomorph.2025.110043.

Tisserand, A., Malaizé, B., Jullien, E., Zaragosi, S., Charlier, K., Grousset, F., 2009. African monsoon enhancement during the penultimate glacial period (MIS 6.5 ~ 170 ka) and its atmospheric impact. Paleoceanography 24. https://doi.org/10.1029/2008pa001630.

Trippetta, F., Petricca, P., Billi, A., Collettini, C., Cuffaro, M., Lombardi, A.M., Scrocca, D., Ventura, G., Morgante, A., Doglioni, C., 2019. From mapped faults to fault-length earthquake magnitude (FLEM): a test on Italy with methodological implications. Solid Earth 10, 1555–1579. https://doi.org/10.5194/se-10-1555-2019.

Turney, C.S.M., Jones, R.T., McKay, N.P., van Sebille, E., Thomas, Z.A., Hillenbrand, C.-D., Fogwill, C.J., 2020. A global mean sea surface temperature dataset for the Last Interglacial (129–116 ka) and contribution of thermal expansion to sea level change. Earth Syst. Sci. Data 12, 3341–3356. https://doi.org/10.5194/essd-12-3341-2020.

Varzi, A.G., Meschis, M., Fallati, L., Scicchitano, G., De Santis, V., Scardino, G., Basso, D., Bracchi, V.A., Savini, A., 2024. New chronology for submerged relict paleoshorelines and associated rates of crustal vertical movements offshore the Marzamemi village, Sicily (Southern Italy). Mar. Geol. 474. https://doi.org/10.1016/j.margeo.2024.107326.

Viger, A., Dominguez, S., Mazzotti, S., Peyret, M., Henriquet, M., Barreca, G., Monaco, C., Damon, A., 2024. Interseismic and long-term deformation of southeastern Sicily driven by the Ionian slab roll-back. Solid Earth 15, 965–988. https://doi.org/10.5194/se-15-965-2024.

Watanabe, M., Goto, K., Imamura, F., Kennedy, A., Sugawara, D., Nakamura, N., Tonosaki, T., 2019. Modeling boulder transport by coastal waves on cliff topography: case study at Hachijo Island, Japan. Earth Surf. Process. Landf. 44, 2939–2956. https://doi.org/10.1002/esp.4684.

Wells, D., Coppersmith, K., 1994. New empirical relationships among magnitude, rupture length, rupture Width, rupture area, and surface displacement. Bull. Seismol. Soc. Am. 84, 974–1002.

Westaway, R., 1993. Quaternary uplift of southern Italy. J. Geophys. Res. Solid Earth 98, 21741–21772. https://doi.org/10.1029/93JB01566.

Whitham, G.B., 1974. Linear and Nonlinear Waves. Wiley, New York.

Williams, D.M., Hall, A.M., 2004. Cliff-top megaclast deposits of Ireland, a record of extreme waves in the North Atlantic-storms or tsunamis? Mar. Geol. 1 (4), 101–117. https://doi.org/10.1016/j.margeo.2004.02.002.

Yeung, N.K.-H., Menviel, L., Meissner, K.J., Taschetto, A.S., Ziehn, T., Chamberlain, M., 2021. Land–sea temperature contrasts at the last Interglacial and their impact on the hydrological cycle. Clim. Past 17, 869–885. https://doi.org/10.5194/cp-17-869-2021.